Supplementary Information for

Efficient and stable industrial-size perovskite/silicon tandems with long-span bisphosphonic self-assembled molecules

Rui Xia†, Jiakai Gu†, Zongyuan Yang†, Lei Gao†, Hongjiang Li†, Hao Wang, Yan Wang, Zongwen Ma, Xueping Zong, Chenyue Wang, Wentao Tang, Xuandi Zhu, Ye Xu, Zhou Liu, Rui He, Hongxu Zhang, Yi Mo, Li Yin, Yujie Liu, Tao Guo, Changhuai Zhu, Cong Zhao, Hongzhuang Ma, Tianyu Teng, Qin Cao, Zhenkun Liu, Dongdong Yan, Chunfeng Zhang, Biao Cui, Guangtao Yang, Xueling Zhang, Shaocong Hou, Zhihui Wang, Zhigang Xie, Yifeng Chen*, Mao Liang*, Lixin Xiao*, Jifan Gao*, Dechun Zou*

Corresponding authors: Yifeng Chen, yifeng.chen01@trinasolar.com; Mao Liang, liangmao717@email.tjut.edu.cn; Lixin Xiao, lxxiao@pku.edu.cn; Jifan Gao, jifan.gao@trinasolar.com; Dechun Zou, dczou@pku.edu.cn

Table-of-contents

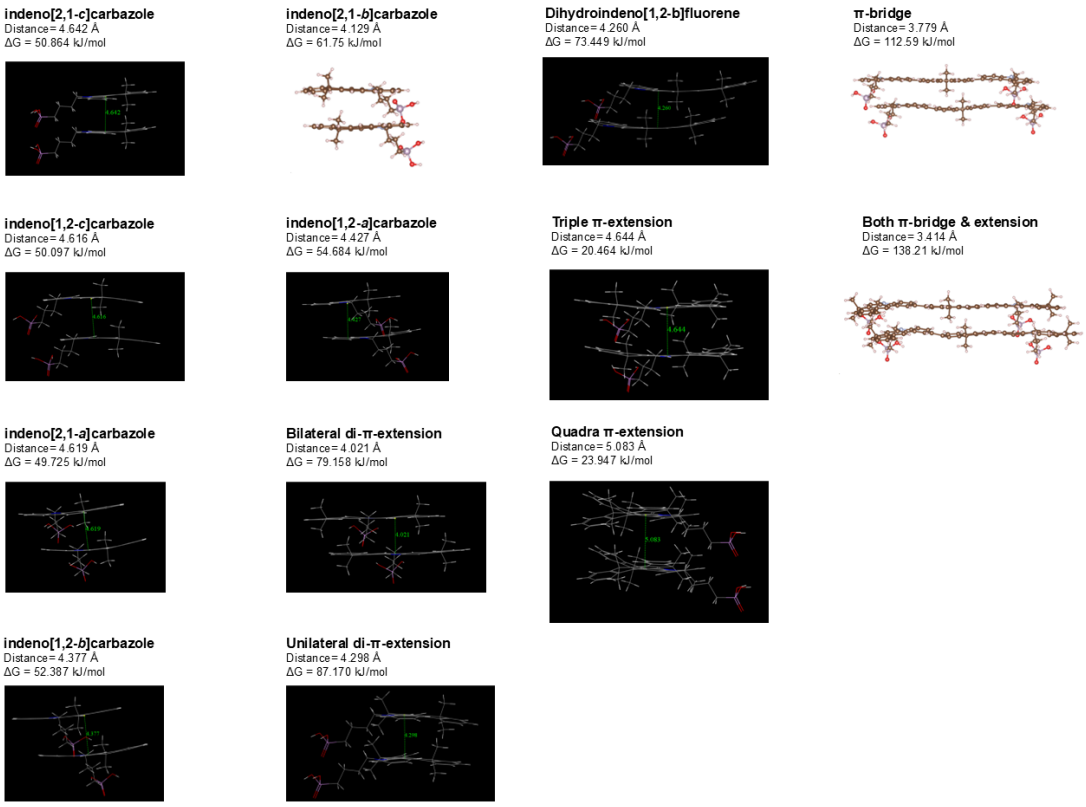

Supplementary Fig. 1 The calculation results of density functional theory (DFT)-driven screening. The influence of different π-conjugated isomers, π-strategies, and the degrees of π-extension on the SAMs' intermolecular interactions and distances.

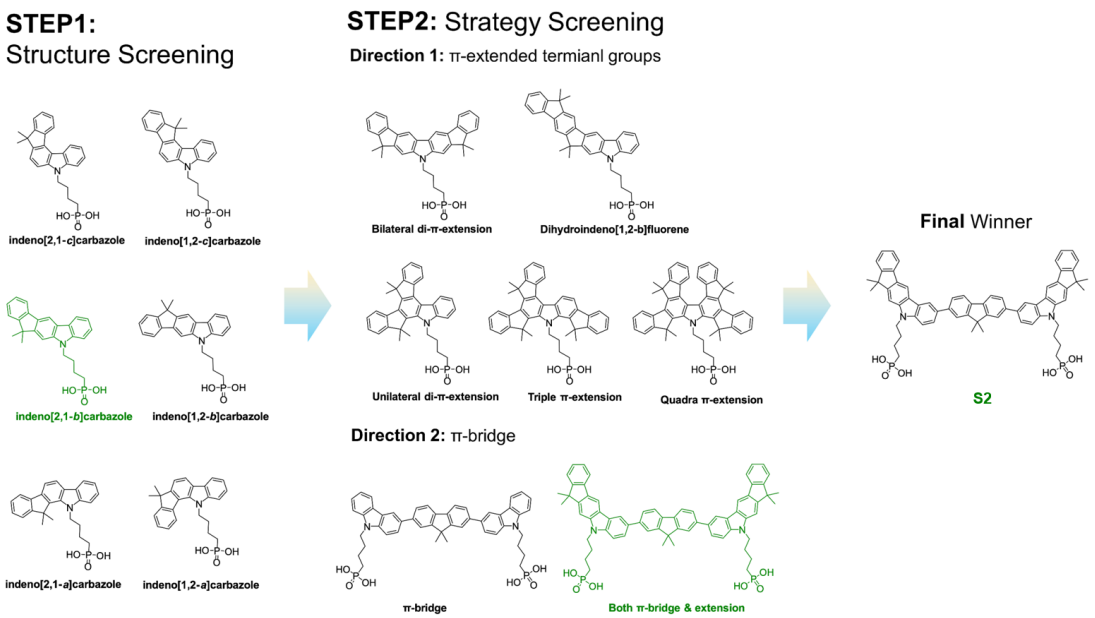

Supplementary Fig. 2 DFT-driven screening workflow. The optimal structure building block (Step 1) and molecular design strategy (Step 2).

Supplementary Note 1. Synthesis of S2 ((((9,9-dimethyl-9H-fluorene-2,7-diyl)bis(7,7-dimethylindeno[2,1-b]carbazole-2,5(7H)-diyl))bis(butane-4,1-diyl))bis(phosphonic acid))

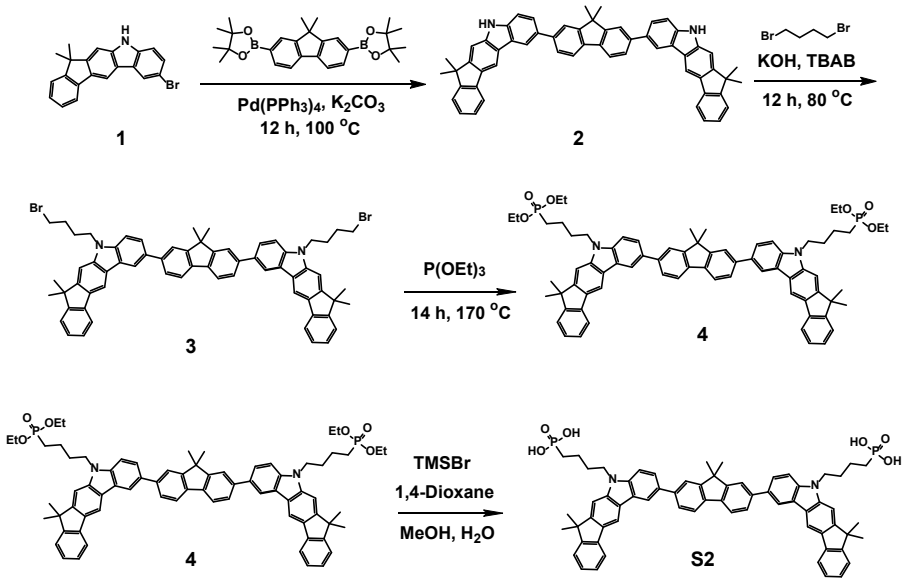

Scheme 1. Synthetic route of **S2**.

Materials for the synthesis of molecules

7,7-Dimethyl-5,7-dihydroindeno[2,1-b]carbazole, acetonitrile (ACN), N-bromosuccinimide (NBS), dichloromethane (CH_2Cl_2), anhydrous sodium sulfate (Na_2SO_4), petroleum ether, 2,2'-(9,9-dimethyl-9H-fluorene-2,7-diyl)bis(4,4,5,5-tetramethyl-1,3,2-dioxaborolane), tetrakis(triphenylphosphine) palladium ($Pd(PPh_3)_4$), toluene, potassium carbonate (K_2CO_3), ethyl alcohol, 1,4-dibromobutane, tertbutyl ammonium bromide, potassium hydroxide (KOH), triethyl phosphite ($P(OEt)_3$), ethyl acetate, 1,4-diethylene dioxide, trimethylsilyl bromide (TMSBr), methyl alcohol. All reagents were used as received from commercial sources without further purification unless otherwise mentioned.

Synthesize of molecule **2**

2,2'-(9,9-dimethyl-9H-fluorene-2,7-diyl)bis(4,4,5,5-tetramethyl-1,3,2-dioxaborolane) (1 g, 2.24 mmol), $Pd(PPh_3)_4$ (0.26 g, 0.22 mmol), and molecule **1** (1.95 g, 5.38 mmol) were dissolved in toluene. K_2CO_3 (2.5 g, 18.09 mmol), H_2O (4 g), and ethyl alcohol (4 g) were added and the mixture was stirred for 12 h at 100℃. Remove the precipitate by filtering and retain the filtrate, then the filtrate was extracted by

CH_2Cl_2, the combined organic phase was dried over anhydrous Na_2SO_4. The crude product was carried forward to the next step without purification.

Synthesize of molecule **3**

Molecule **2** (1.07 g, 1.41 mmol) was dissolved in 1,4-dibromobutane (15.22 g, 70.5 mmol). Tertbutyl ammonium bromide (0.09 g, 0.28 mmol), KOH (1.74 g, 31.10 mmol) and H_2O (1.74 g) were then added in sequence. The mixture was stirred at 80℃ for 12 h. All reactions were performed under argon atmosphere. Then the mixture was extracted by CH_2Cl_2. The combined organic phase was dried over anhydrous Na_2SO_4, and concentrated under reduced pressure. The crude product was purified by column chromatography using petroleum ether: CH_2Cl_2 = 5:2 as eluent to afford Molecule **3** (1.11 g, yield: 76.55%) as a white solid.^{1}H NMR (400 MHz, $CDCl_3$) δ 8.52 (d, *J* = 17.9 Hz, 4H), 7.94 – 7.87 (m, 6H), 7.84 (dd, *J* = 8.4, 1.6 Hz, 2H), 7.79 (d, *J* = 7.7 Hz, 2H), 7.51 (dd, *J* = 7.8, 4.8 Hz, 4H), 7.48 – 7.40 (m, 4H), 7.33 (t, *J* = 7.2 Hz, 2H), 4.47 (s, 4H), 3.49 (t, *J* = 6.4 Hz, 4H), 2.24 – 2.14 (m, 4H), 2.05 (dd, J = 15.0, 6.4 Hz, 4H), 1.75 (s, 6H), 1.65 (s, 12H). ^{13}C NMR (101 MHz, $CDCl_3$) δ 154.5, 153.1, 141.1, 140.1, 139.8, 137.5, 132.9, 131.6, 127.0, 126.3, 126.1, 125.0, 123.7, 122.6, 121.5, 120.2, 119.2, 118.8, 111.6, 108.8, 102.8, 47.1, 46.7, 42.4, 33.2, 32.5, 30.9, 30.2, 28.1, 27.5.

Synthesize of molecule **4**

Molecule **3** (1.11 g, 1.08 mmol) was dissolved in $P(OEt)_3$ (8.97 g, 54 mmol). The mixture was heated at 170℃ for 14 h under argon atmosphere. The solvent was removed under reduced pressure. The crude product was purified by column chromatography using ethyl acetate as eluent to afford Molecule **4** (1.15 g, yield: 93.50%) as a transparent oil liquid.^{1}H NMR (400 MHz, DMSO-d_6) δ 8.73 (s, 2H), 8.65 (s, 2H), 8.05 (s, 2H), 7.97 (d, *J* = 7.9 Hz, 2H), 7.92 (d, *J* = 7.6 Hz, 2H), 7.87 (d, *J* = 9.3 Hz, 4H), 7.82 (d, *J* = 8.8 Hz, 2H), 7.74 (d, *J* = 8.6 Hz, 2H), 7.56 (d, *J* = 7.5 Hz, 2H), 7.38 (t, *J* = 7.4 Hz, 2H), 7.28 (t, *J* = 7.4 Hz, 2H), 4.52 (d, *J* = 6.1 Hz, 4H), 3.94 – 3.85 (m, 8H), 1.99 – 1.90 (m, 4H), 1.84 – 1.76 (m, 4H), 1.69 (s, 6H), 1.57 (s, 16H), 1.14 (t, *J* = 7.0 Hz, 12H). ^{13}C NMR (101 MHz, DMSO-d_6) δ 154.9, 153.4, 153.2, 141.5, 140.7, 140.4, 139.9, 137.3, 132.0, 131.1, 127.5, 126.6, 126.2, 124.9, 123.7, 123.3, 122.3, 121.5, 120.9, 119.6, 118.7, 112.3, 110.3, 104.5, 61.2, 47.2, 46.8, 42.5, 29.8, 28.2, 27.6, 25.4, 24.1, 20.2, 16.7.

Synthesize of molecule **S2**

Molecule **4** (1.15 g, 1.01 mmol) was dissolved in anhydrous 1,4-diethylene dioxide (8 mL), TMSBr (3.16 g, 20.64 mmol) was slowly added and the mixture was stirred for

24 h at room temperature under argon atmosphere. 5 mL of methyl alcohol was then added. After stirring for 3 h at room temperature, the mixture was concentrated under reduced pressure and the remaining liquid was dissolved in 1.5 mL methyl alcohol. 50 mL of distilled water was added dropwise until the solution became turbid. The product was collected by filtration, and washed with water to give S2 (0.87 g, yield: 83.65%) as a light pink solid.^{1}H NMR (400 MHz, DMSO-d_6) δ 8.73 (s, 2H), 8.65 (s, 2H), 8.06 (s, 2H), 7.97 (d, J = 7.9 Hz, 2H), 7.92 (d, J = 7.6 Hz, 2H), 7.87 (s, 4H), 7.82 (d, J = 7.9 Hz, 2H), 7.73 (d, J = 8.6 Hz, 2H), 7.56 (d, J = 7.5 Hz, 2H), 7.38 (t, J = 7.4 Hz, 2H), 7.28 (t, J = 7.4 Hz, 2H), 4.51 (s, 4H), 1.94 (d, J = 6.7 Hz, 4H), 1.71 (d, J = 13.1 Hz, 6H), 1.65 (dd, J = 9.2, 6.5 Hz, 8H), 1.56 (d, J = 12.2 Hz, 12H). ^{13}C NMR (151 MHz, DMSO-d_6) δ 154.9, 153.5, 153.2, 141.5, 140.77, 140.4, 139.9, 137.3, 131.9, 131.1, 127.5, 126.5, 126.2, 125.0, 123.5, 123.1, 122.4, 121.5, 120.9, 119.6, 118.7, 112.3, 110.2, 104.5, 47.2, 46.8, 42.8, 30.0, 28.2, 27.6, 27.3, 25.6, 16.8. HRMS-ESI (m/z): {[M-2H]$^{2-}$} / 2 Calcd. for ($C_{65}H_{62}N_2O_6P_2$): 513.1963, found: 513.1968.

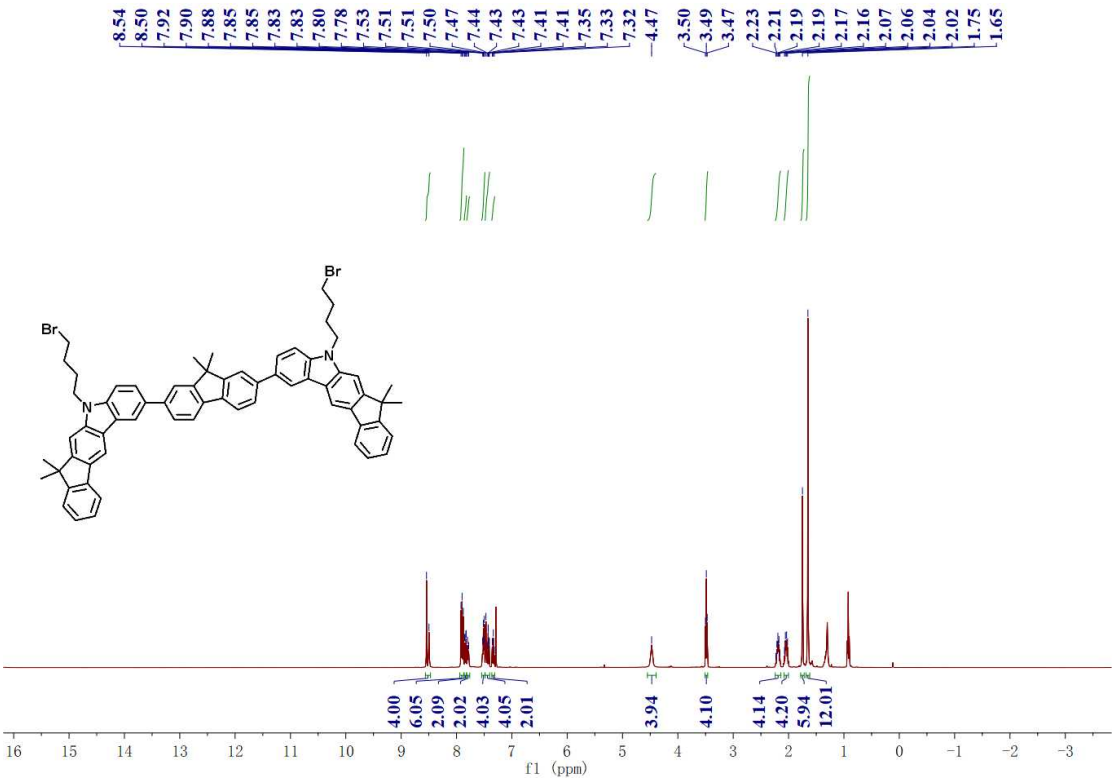

Supplementary Fig. 3 ^{1}H NMR spectrum of compound **3** in $CDCl_3$.

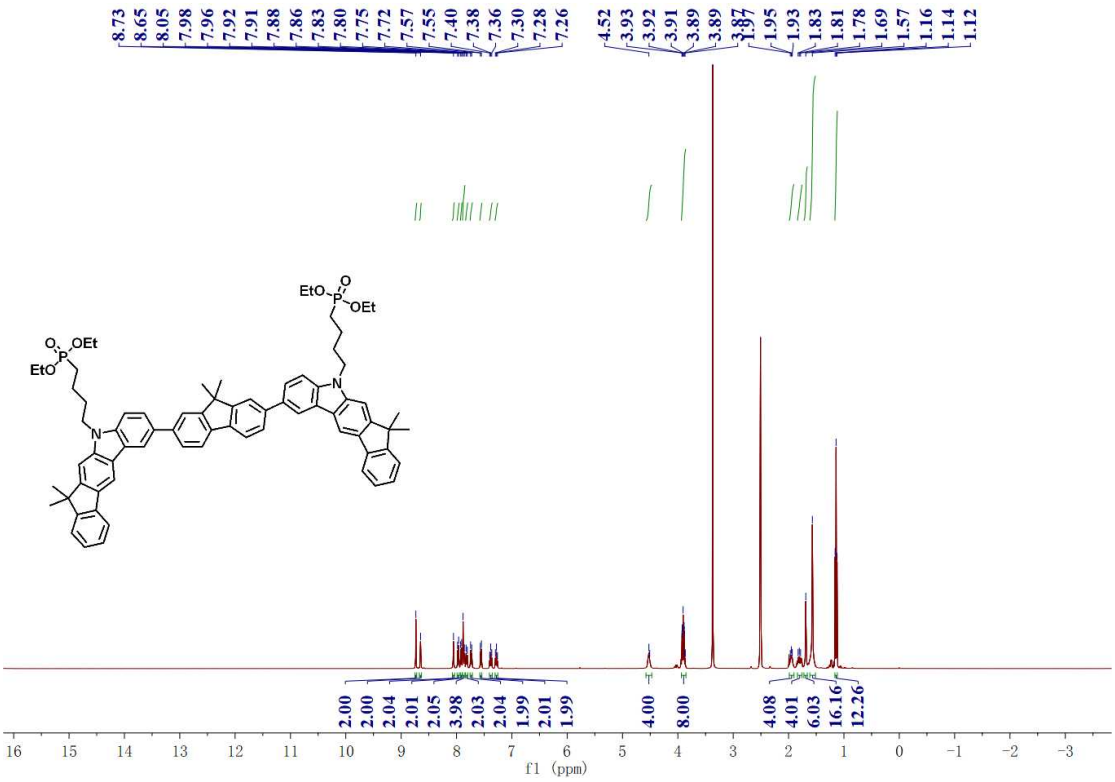

Supplementary Fig. 4 ^{1}H NMR spectrum of compound **4** in DMSO-d_6.

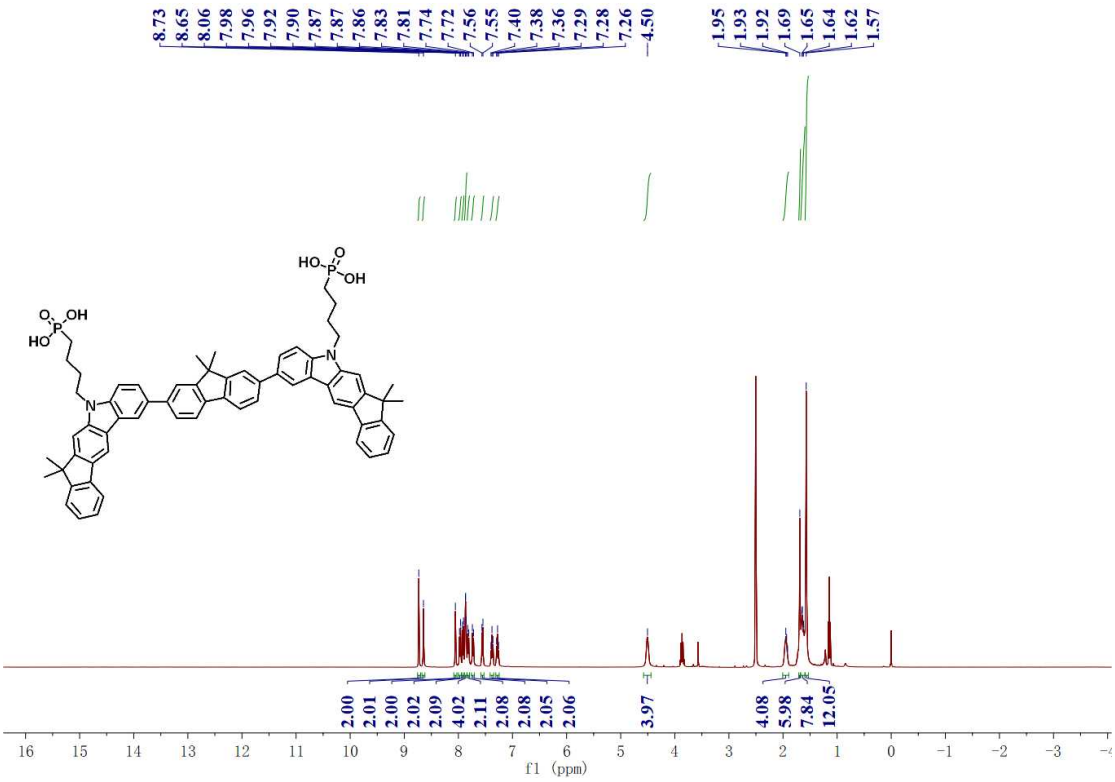

Supplementary Fig. 5 ^{1}H NMR spectrum of compound S2 in DMSO-d_6.

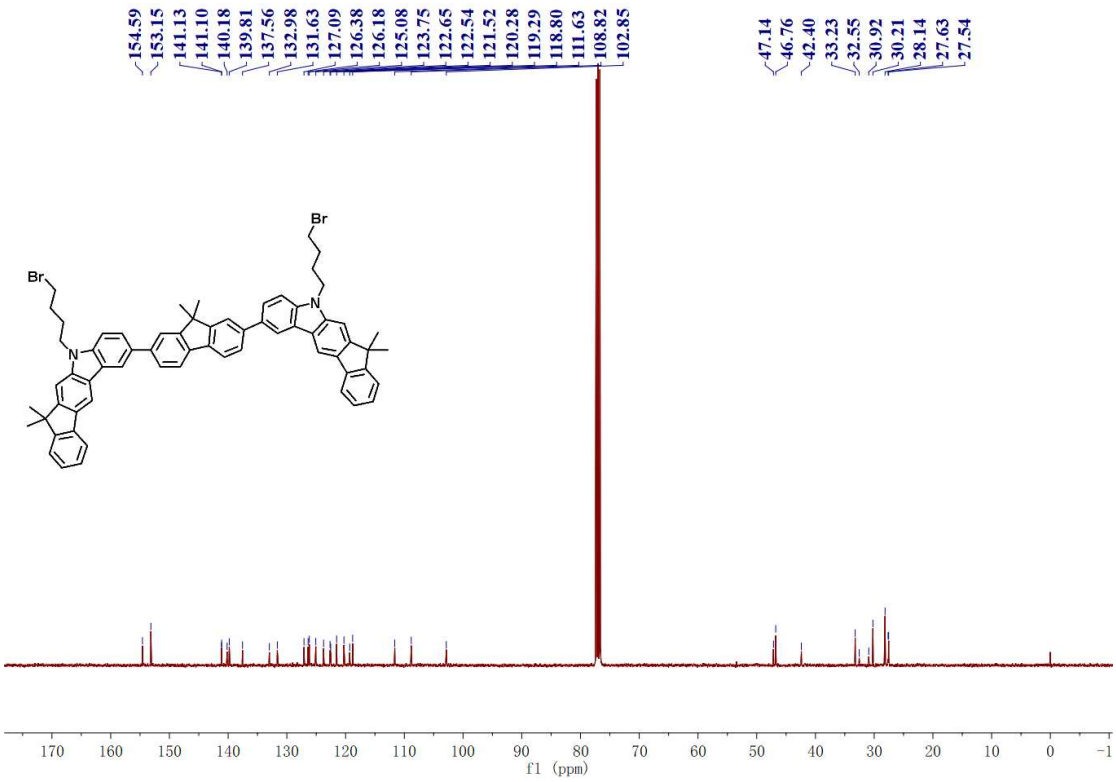

Supplementary Fig. 6 ^{13}C NMR spectrum of compound **3** in $CDCl_3$.

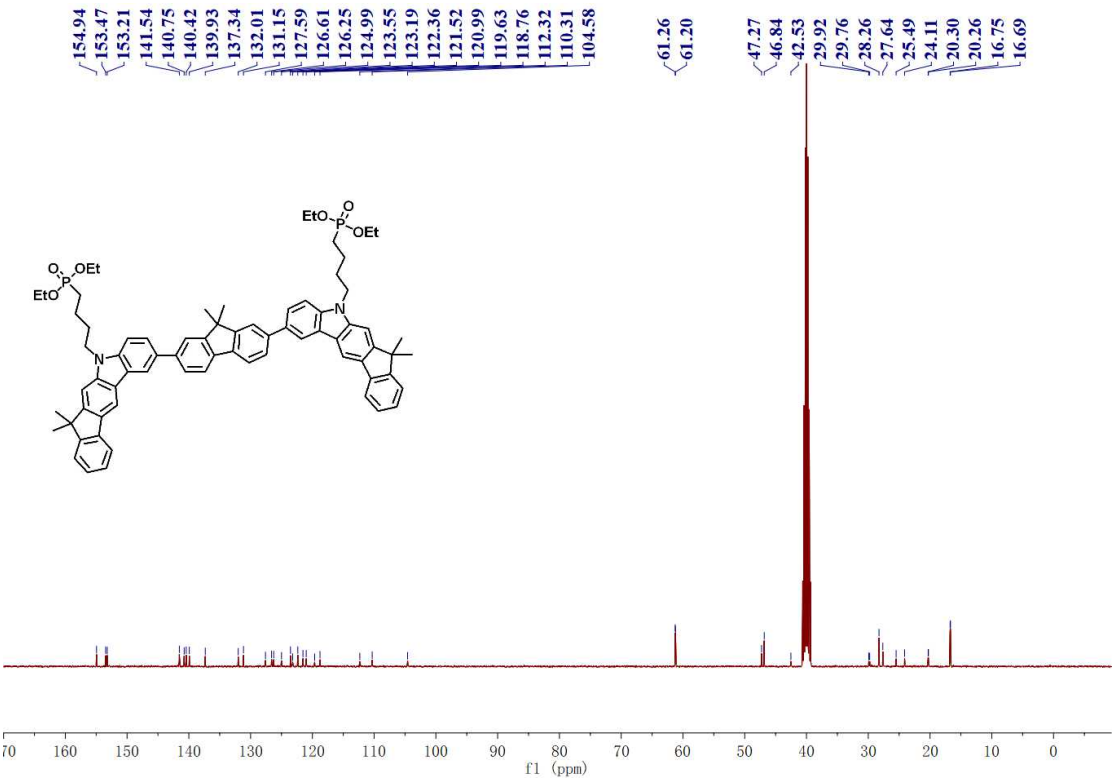

Supplementary Fig. 7 ^{13}C NMR spectrum of compound **4** in DMSO-d_6.

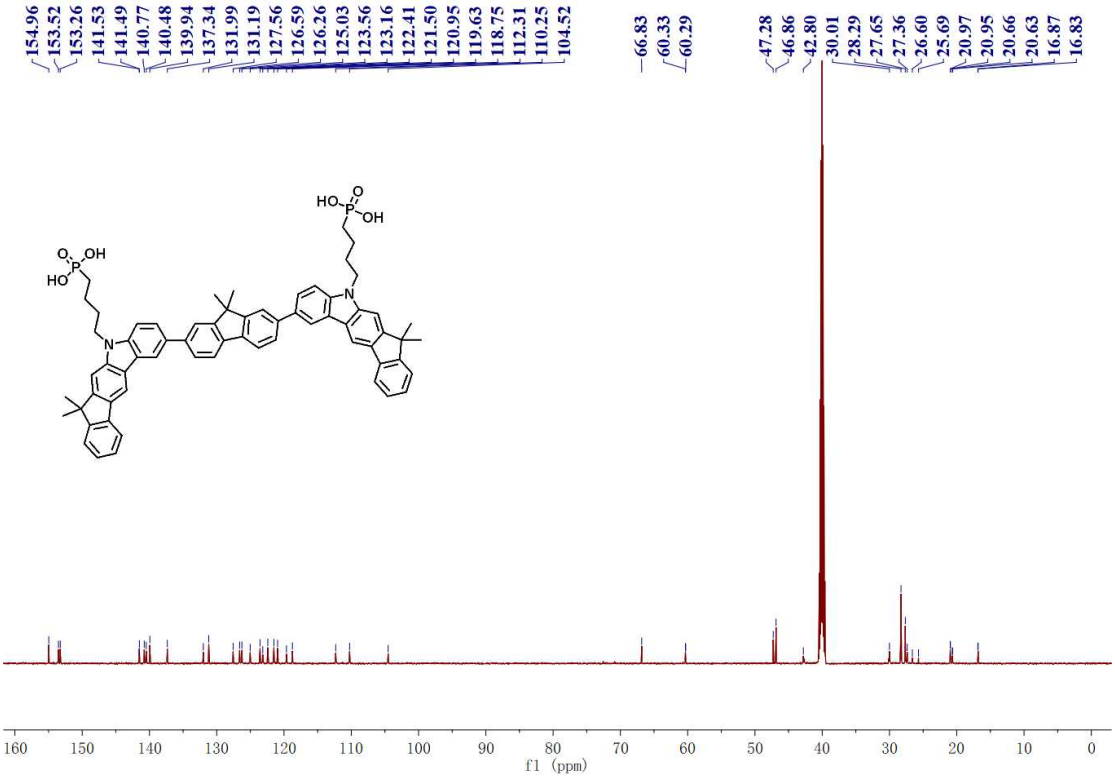

Supplementary Fig. 8 ^{13}C NMR spectrum of compound **S2** in DMSO-d_6.

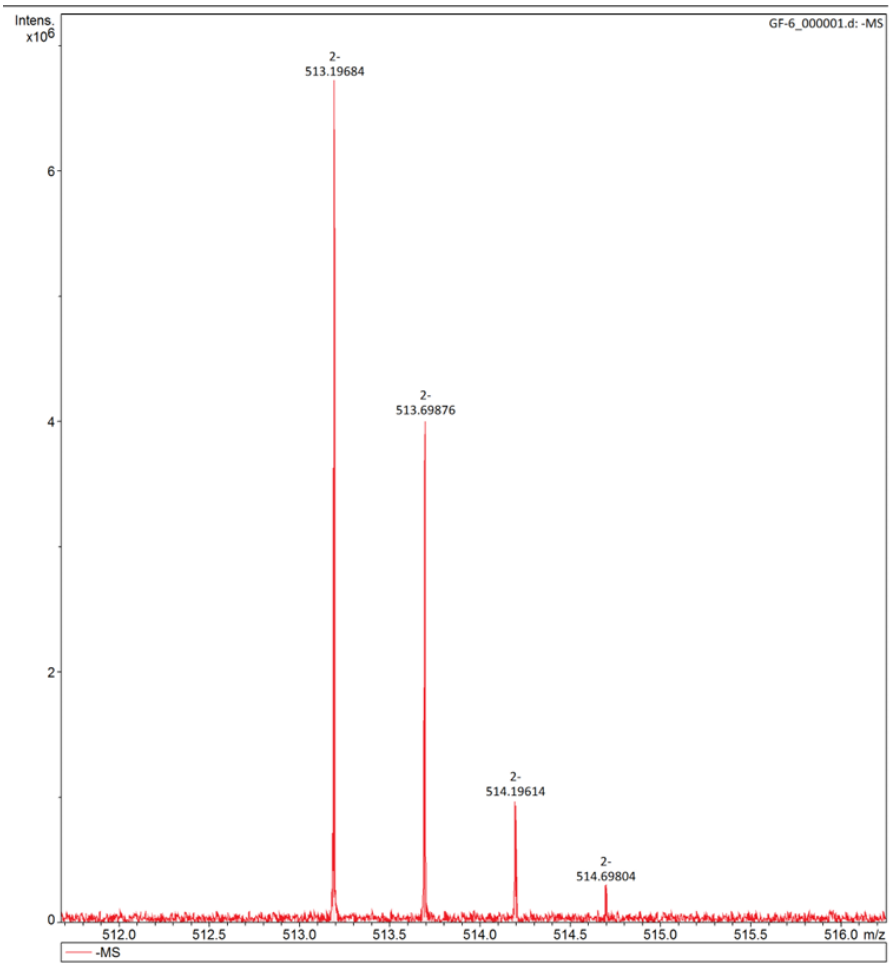

Supplementary Fig. 9 HRMS spectrum of **S2**. (m/z = (M-2)/2).

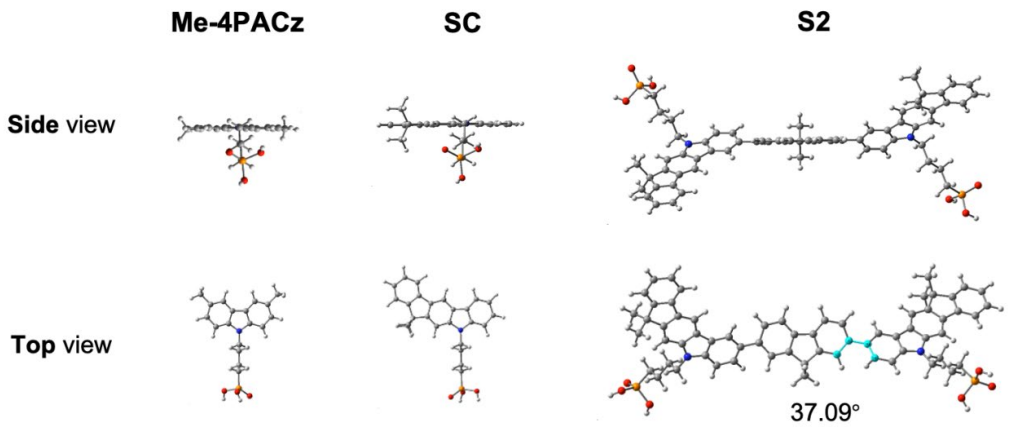

Supplementary Fig. 10 Monomer geometric structures of Me-4PACz, **SC** and **S2**. (Side-view and Top-view)

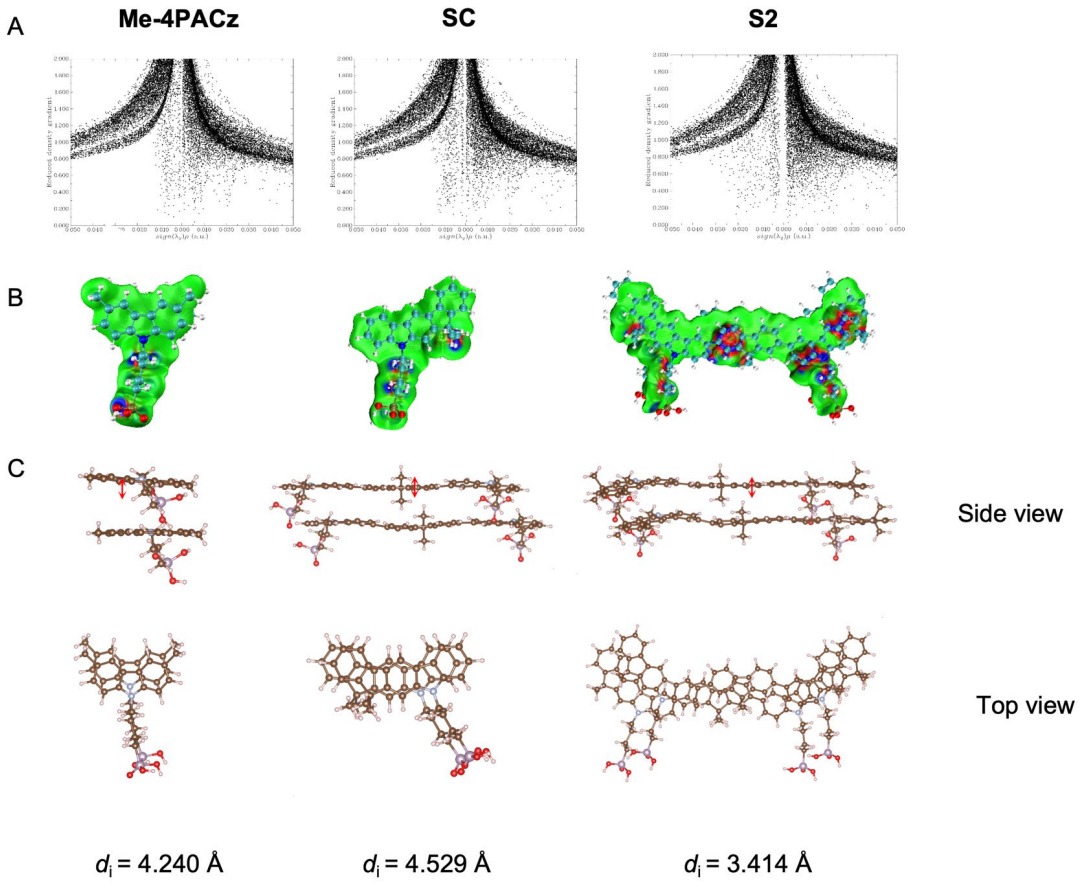

Supplementary Fig. 11 Reduced density gradient (RDG) analysis, Hirshfeld independent gradient model (IGMH) visualization, and calculated intermolecular distances (d_i) for the dimers of (A) Me-4PACz, (B) **SC**, and (C) **S2**. The progressively increased population of points in the negative sign (λ_2) ρ region indicates strengthened attractive intermolecular interactions upon molecular expansion from Me-4PACz, **SC** to **S2**. Correspondingly, the increasingly extensive green isosurfaces characteristic of attractive π–π and van der Waals interactions valid the enhanced interaction region. The π-extended terminal of **S2** strengthens the inter-molecular π-π interactions, leading to the shorter intermolecular distances than that of Me-4PACz and **SC**. Meanwhile, the gem-dimethyl groups on the indenocarbazole units and the two methyl groups on the central fluorene create steric effects (red regions)that prevent excessive aggregation.

Supplementary Note 2. Molecular dynamics (MD) simulations of the structural evolution of different SAMs.

Systems containing 30 molecules of each species (Me-4PACz, **SC**, and **S2**) were constructed based on energy-minimized three-dimensional geometries. Atom types and partial charges were assigned using the GAFF force field. Each system was placed in an independent cubic simulation box constructed in GROMACS 2025, followed by steepest descent minimisation to eliminate unfavorable contacts and a 100 ps NVT pre-equilibration to stabilize the system at the target temperature. Production simulations were then performed for 100 ns with a 2 fs leap-frog integration time-step under periodic boundary conditions at 373 K, controlled by a V-rescale thermostat (τ = 0.1 ps). Long-range electrostatic interactions were treated using the particle-mesh Ewald (PME) method with a real-space cut-off of 1.0 nm, while van der Waals interactions were described by Lennard-Jones potentials with the same cut-off distance and standard dispersion corrections applied for long-range contributions. All bonds involving hydrogen atoms were constrained using the LINCS algorithm. Accessible surface areas (ASA) were calculated every 50 ps using a 0.14 nm probe to monitor the time-dependent aggregation behavior of molecules[1].

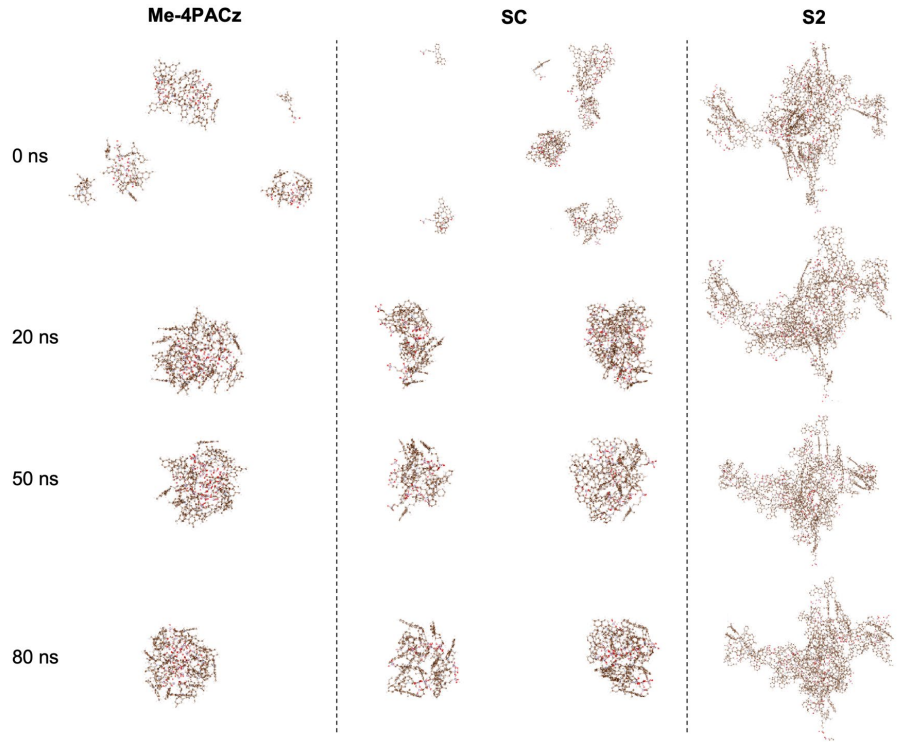

Supplementary Fig. 12 Successive snapshots from MD simulations of 30 Me-4PACz monomers (A), **SC** (B) , and **S2** (C). All of the snapshots were view from the a-axis direction.

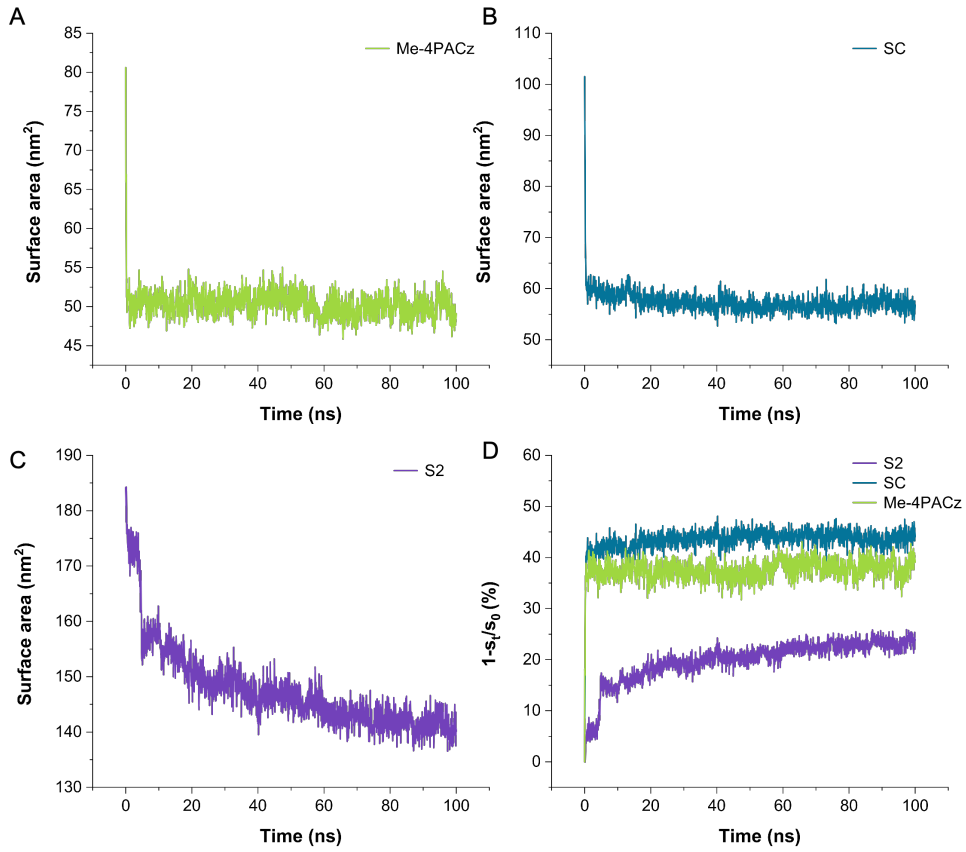

Supplementary Fig. 13 Quantitatively analysis aggregation by tracking the ASA value of (A) Me-4PACz, (B) **SC**, and (C) **S2**. (D) The aggregation degree calculated from 1-s_t/s_0,where s_t is the ASA value at time t and s_0 is the initial ASA at $t = 0$. The simulations revealed a fundamental divergence in self-organization behavior. The 4PACz system underwent rapid reconstruction and 30 initially random dispersed monomers spontaneously aggregate into a closely packed cluster within the first 10 ns, driven by strong π-π interactions. In contrast, **S2** molecules remained spatially dispersed throughout the 100 ns trajectory, demonstrating a robust resistance to agglomeration. The Me-4PACz system exhibited a significant decrease of 39.07% in ASA (from 80.59 nm^2 to 49.10 nm^2). The **SC** system exhibited a significant decrease of 44.03% in ASA (from 101.49 nm^2 to 56.80 nm^2). By contrast, **S2** system reached a stable state after ~ 40 ns with a substantially lower decrease of 23.94% (from 184.2 nm^2 to 140.1 nm^2). These results confirm that molecule design strategy effectively suppresses excessive intermolecular interactions and enhances structural stability under thermal stress. The rotatable single bond linkage provides the necessary conformational adaptability, while the sp^3 hybridized gem-dimethyl groups on the indenocarbazole and fluorene cores introduce a critical steric hinderance that mitigates excessive π-π interaction. Consequently, **S2** forms a thermally stable amorphous-conformal molecular arrangement, ensuring a suppressed aggregation and uniform interfacial contact even

under prolonged thermal stress.

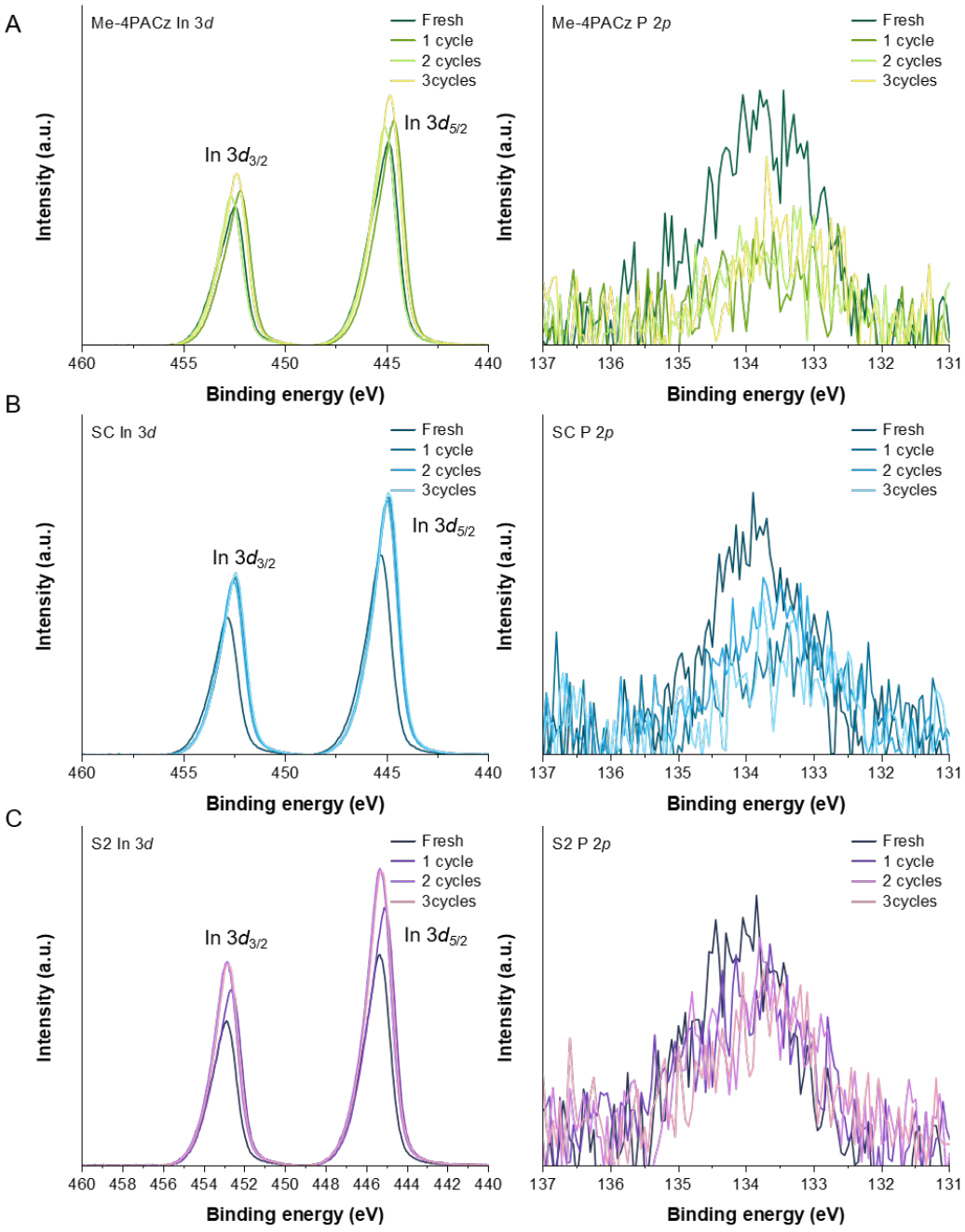

Supplementary Fig. 14 In 3*d* (left) and P 2*p* (right) X-ray photoelectron spectroscopy (XPS) spectra for (A) Me-4PACz/ITO, (B) SC/ITO, and (C) S2/ITO, before and after washing with different cycles of ethanol. The coverage capability was semi-quantitively analyzed by examining the ratio of the P 2*p* peak in the SAMs to the In $3d_{3/2}$ peak in the ITO substrate.

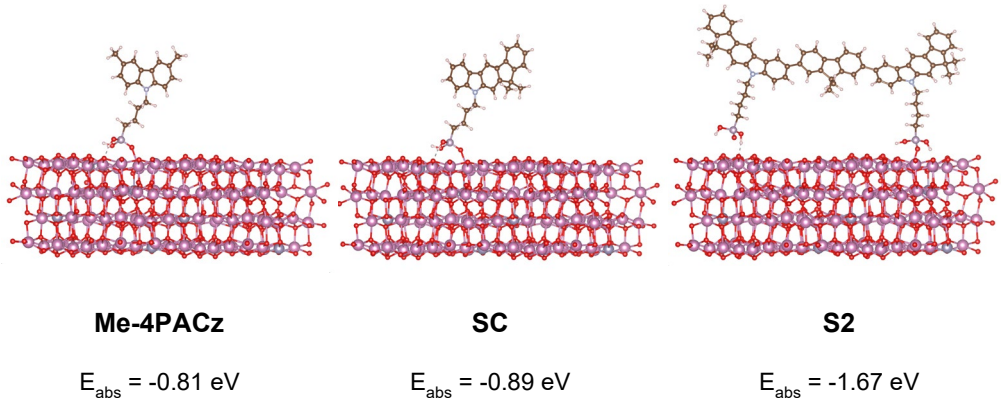

Supplementary Fig. 15 DFT-relaxed structures and calculated adsorption energies of Me-4PACz, **SC**, and **S2** on the surface of ITO (100) substrate. The results demonstrated that **S2** exhibits enhanced coverage ability and more robust binding on the ITO substrate compared to Me-4PACz and **SC**.

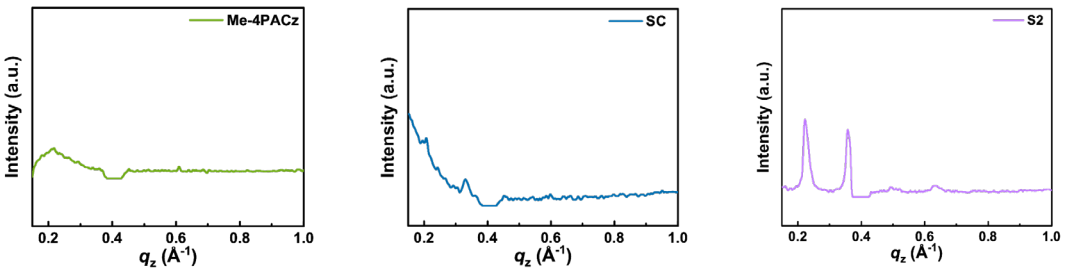

Supplementary Fig. 16 Out-of-plane intensity profile of the corresponding grazing-incidence wide-angle X-ray scattering (GIWAXS) patterns.

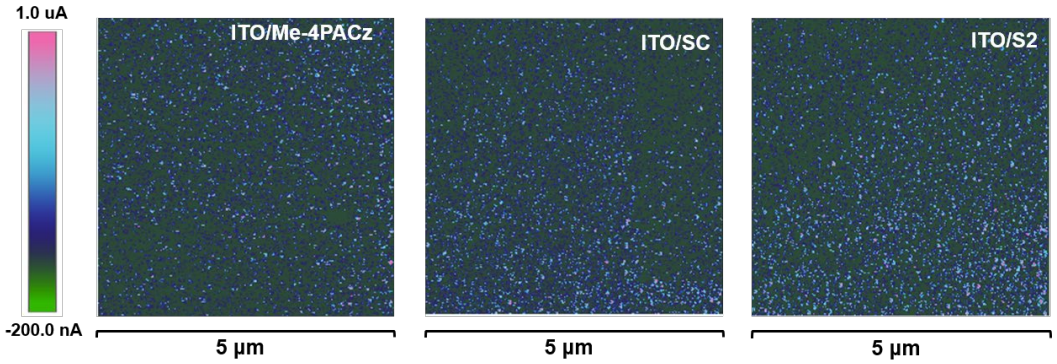

Supplementary Fig. 17 Conductive atomic force microscopy of SAMs on ITO substrate measured at a 20 mV bias.

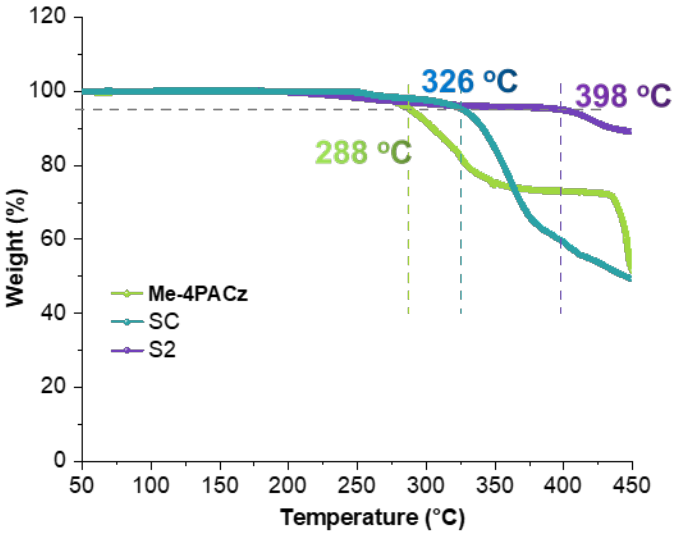

Supplementary Fig. 18 Thermogravimetric analysis (TGA) thermograms of different SAMs.

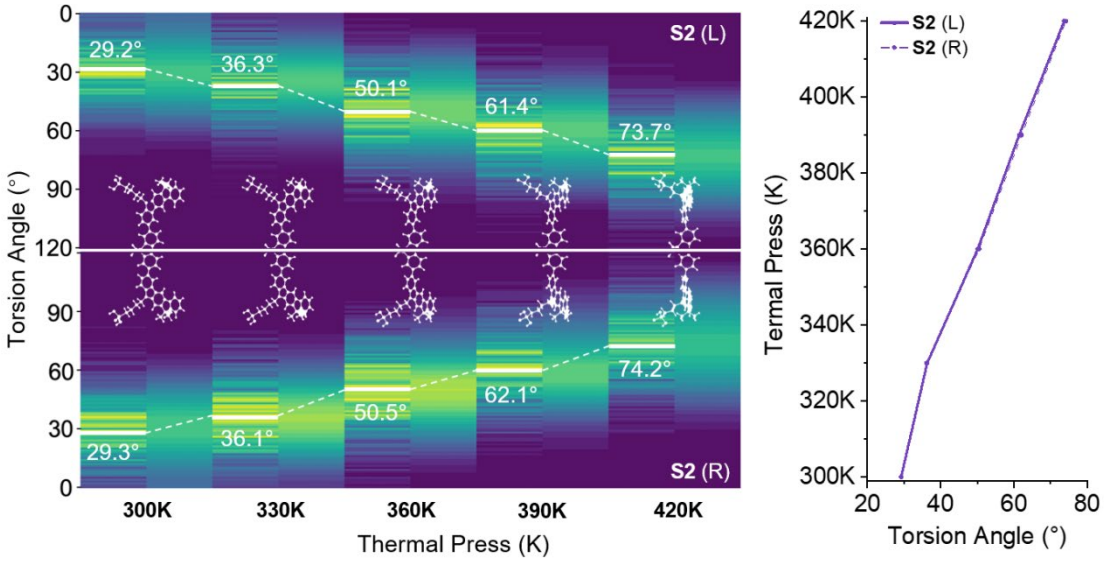

Supplementary Fig. 19 Intramolecular torsion angles as the function of temperature (300 K~420 K) of **S2**.

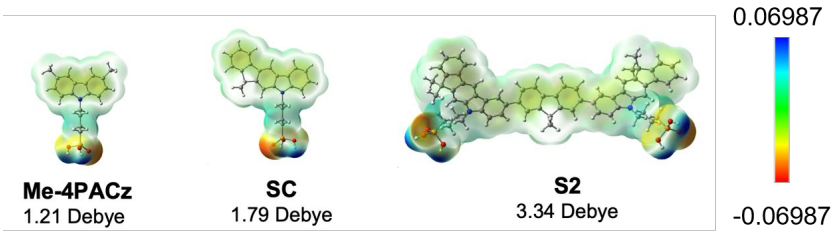

Supplementary Fig. 20 Molecular electrostatic potential maps and dipole moments (in Debye) of Me-4PACz, **SC** and **S2**. Red/blue regions represent negative/positive electrostatic potential.

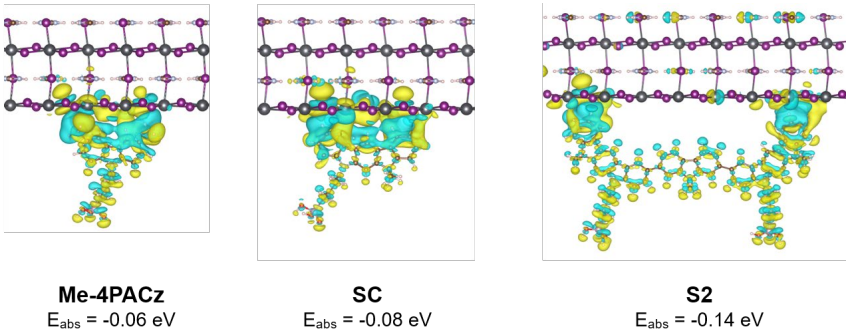

Supplementary Fig. 21 DFT-optimized adsorption structures of Me-4PACz, **SC**, and **S2** on PbI_2-riched $FAPbI_3$ (100) surface with charge density difference maps and adsorption energies. The results demonstrated that **S2**/PVK exhibits a higher binding energy compared to the Me-4PACz and **SC** system, indicating stronger interfacial interactions.

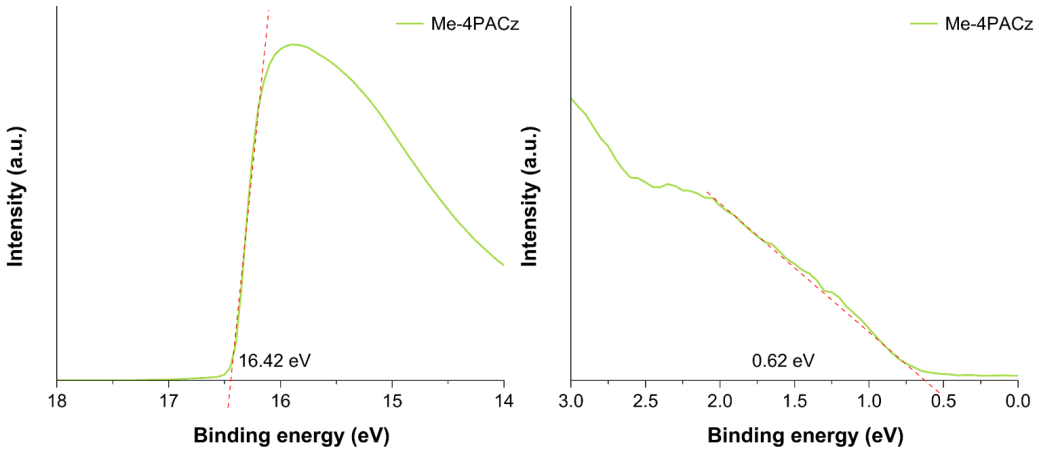

Supplementary Fig. 22 Ultraviolet photoelectron spectroscopy (UPS) spectra of ITO substrates covered by Me-4PACz. Left, UPS spectrum around the secondary electron cut-off (work function). Right, UPS spectrum in the valence-band region.

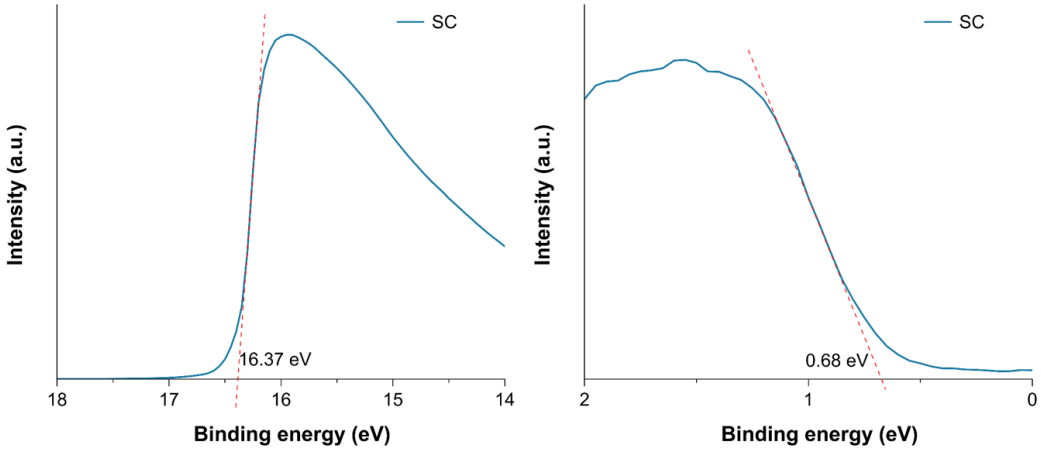

Supplementary Fig. 23 UPS spectra of ITO substrates covered by SC. Left, UPS spectrum around the secondary electron cut-off (work function). Right, UPS spectrum in the valence-band region.

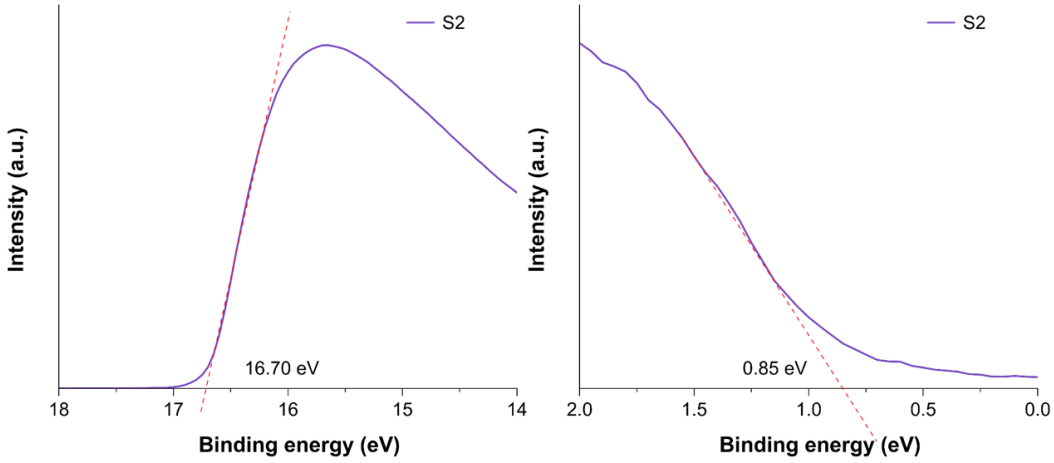

Supplementary Fig. 24 UPS spectra of ITO substrates covered by **S2**. Left, UPS spectrum around the secondary electron cut-off (work function). Right, UPS spectrum in the valence-band region.

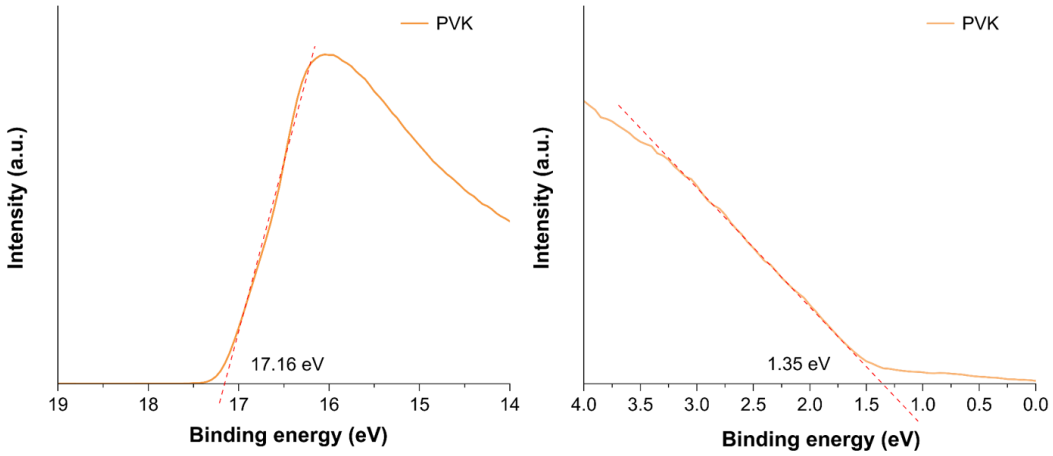

Supplementary Fig. 25 UPS spectra of ITO substrates covered by perovskite film. Left, UPS spectrum around the secondary electron cut-off (work function). Right, UPS spectrum in the valence-band region.

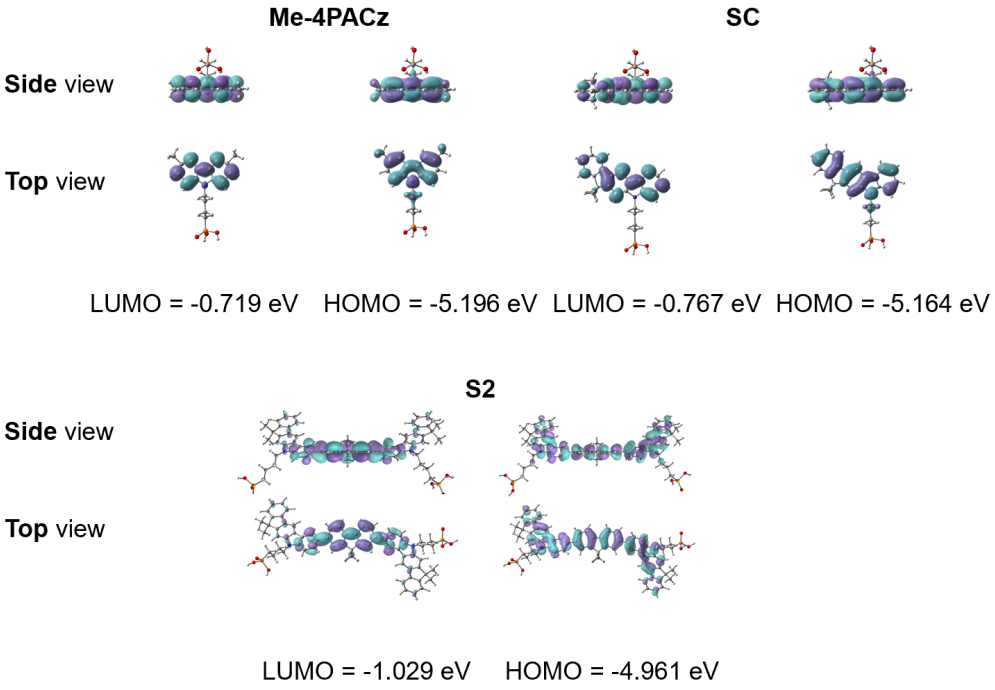

Supplementary Fig. 26 The lowest unoccupied molecular orbital (LUMO)/highest occupied molecular orbital (HOMO) distributions and DFT-calculated energy level of Me-4PACz, **SC** and **S2** (Side-view and Top-view).

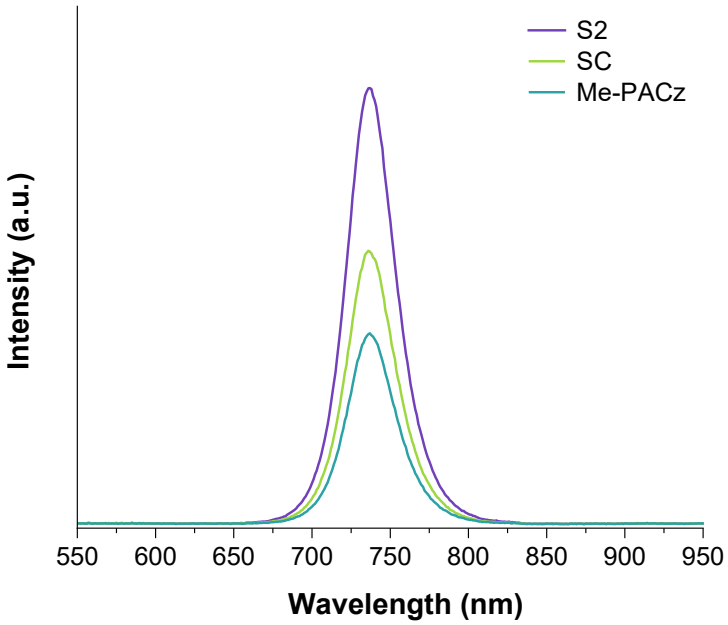

Supplementary Fig. 27 Steady state photoluminescence (PL) spectra of bare perovskite films and perovskite films based on Me-4PACz, **SC**, and **S2** with ITO/SAM/perovskite structure.

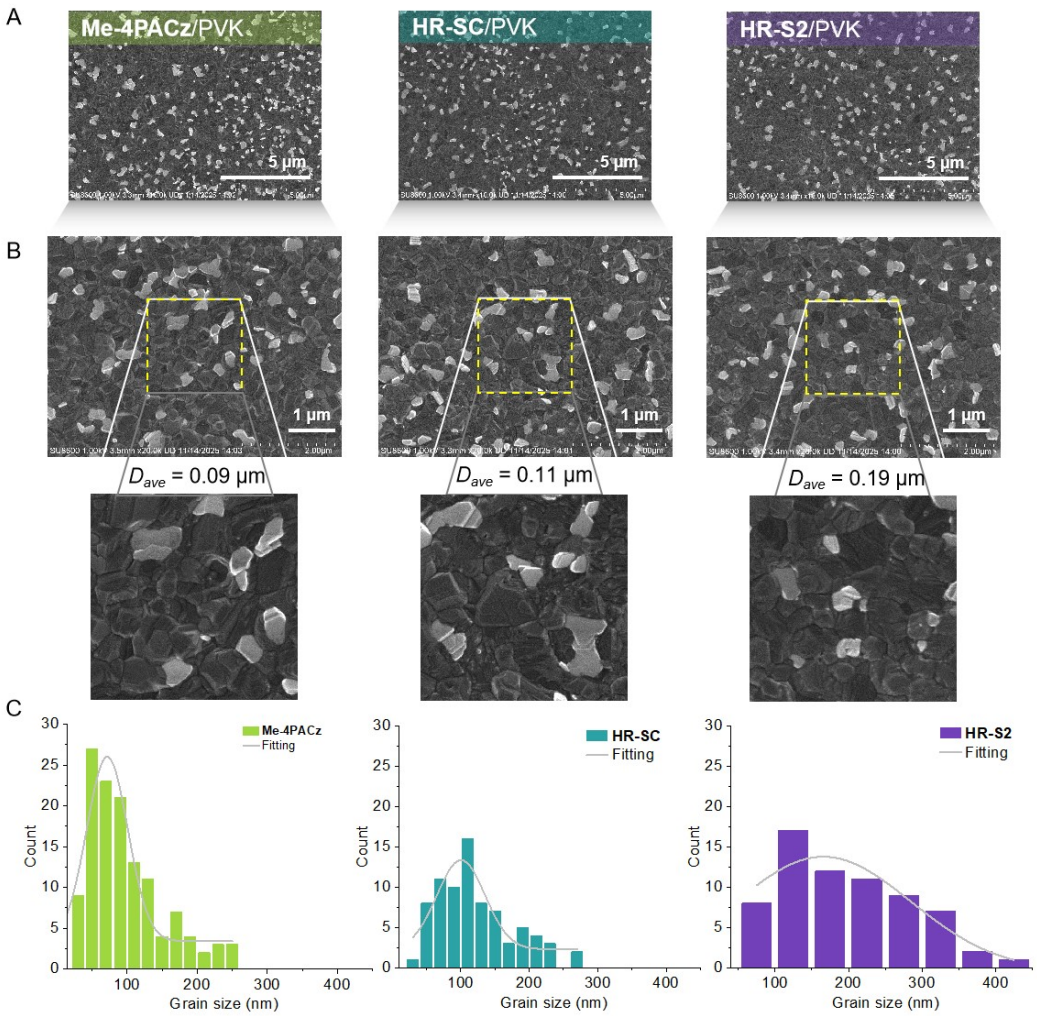

Supplementary Fig. 28 (A,B) Top-view scanning electron microscope (SEM) images of perovskite films coated on different SAMs based on silicon substrate (scale bars: 5 μm in (A) and 1 μm in (B)). (C) Average perovskite grain size of the corresponding SAM/PVK samples.

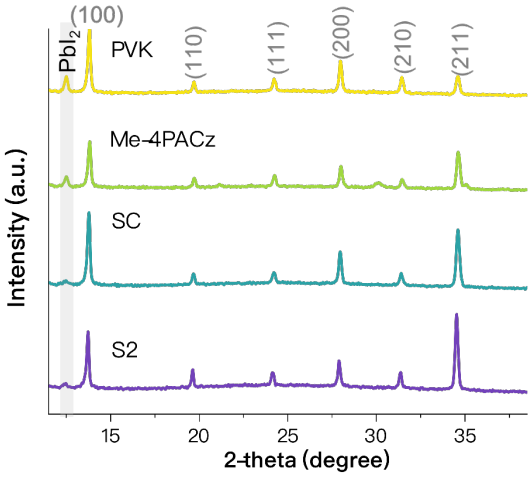

Supplementary Fig. 29 X-ray diffraction patterns of perovskite films deposited on different SAMs.

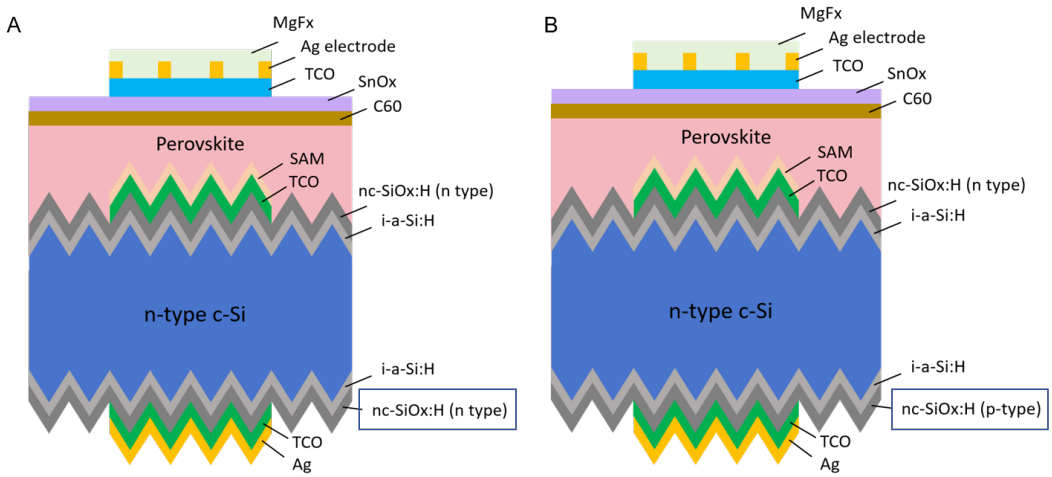

Supplementary Fig. 30 Schematic illustration of the devices based on (A) n-i-n and (B) n-i-p substrate.

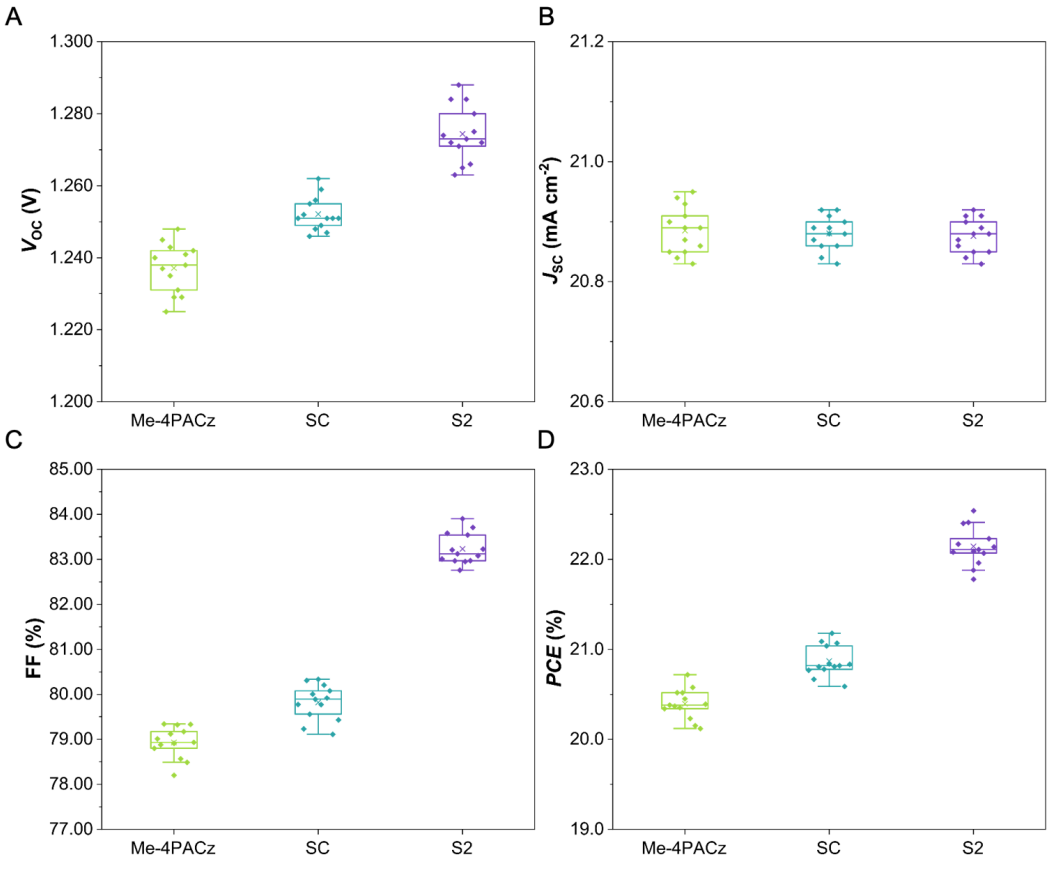

Supplementary Fig. 31 Statistical distribution of (A) open-circuit voltage (V_{OC}), (B) short-circuit current density (J_{SC}), (C) fill factor (FF) and (D) power conversion efficiency (PCE) for n-i-n devices employing various SAMs.

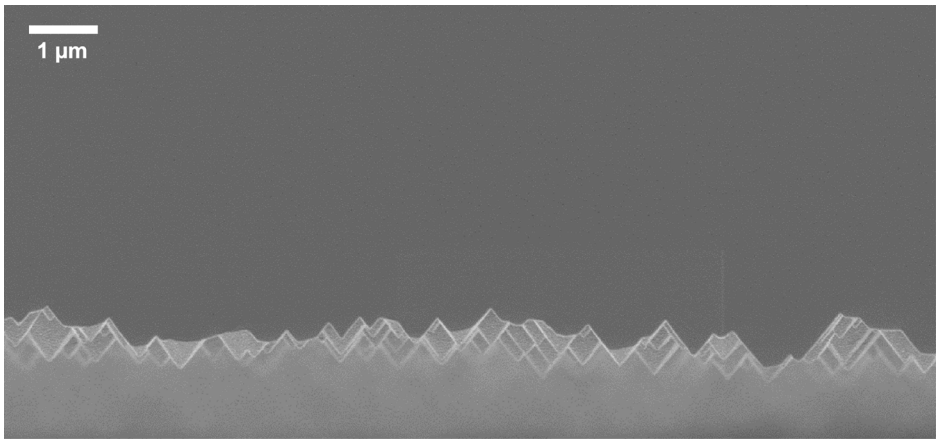

Supplementary Fig. 32 Cross-sectional SEM image of the back side of the silicon bottom cell in TSC.

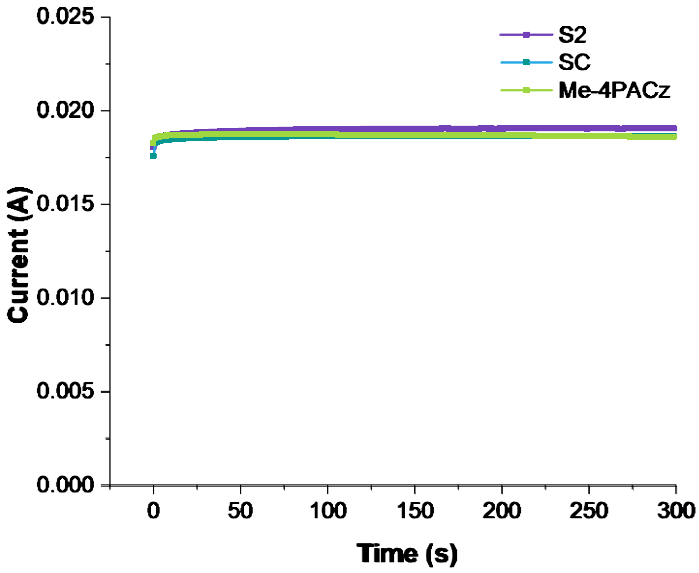

Supplementary Fig. 33 Current-time (*I-t*) curves for lab-scale TSCs based on different SAMs, Me-4PACz (1.70 V, 32.28%), **SC** (1.73 V, 32.91%), and **S2** (1.76 V, 34.29%).

Test and Calibration Center of New Energy Device and Module,
Shanghai Institute of Microsystem and Information Technology,
Chinese Academy of Sciences (SIMIT)

Measurement Report

Report No. 26TR051902

Client Name	Beijing Huairou Laboratory / Trina Solar Co., Ltd
Client Address	No.8, Yangyan 1st East Rd, Huairou District Beijing P.R. China/ No.2 Tianhe Road, Trina PV Industrial Park, Xinbei District, Changzhou City, Jiangsu Province P.R. China
Sample	Perovskite/crystalline silicon two-terminal tandem solar cell
Manufacturer	Beijing Huairou Laboratory / Trina Solar Co., Ltd
Measurement Date	19th May, 2026

Performed by:	Qiang Shi	**Date:** 19/05/2026
Reviewed by:	Wenjie Zhao	**Date:** 19/05/2026
Approved by:	Zhengxin Liu	**Date:** 19/05/2026

Address: No.235 Chengbei Road, Jiading, Shanghai **Post Code:** 201800
E-mail: solarcell@mail.sim.ac.cn **Tel:** +86-021-69976905

Report No. 26TR051902

====Measurement Results ====

	Forward Scan (Isc to Voc)	Reverse Scan (Voc to Isc)	MPP-Tracking
Area		97.15 mm^2	
Isc	20.209 mA	20.192 mA	/
Voc	1.990 V	1.990 V	/
Pmax	32.924 mW	33.162 mW	32.872 mW
Ipm	18.891 mA	18.951 mA	18.843 mA
Vpm	1.743 V	1.750 V	1.745 V
FF	81.86 %	82.51 %	/
Eff	33.89 %	34.13 %	33.84 %

- Designated illumination area defined by a thin mask was measured by measuring microscope.
- MPPT results correspond to the average values obtained during the steady-state period from 331 to 360 s.
- Test results listed in this measurement report refer exclusively to the mentioned measured sample.
- The results apply only at the time of the test, and do not imply future performance.

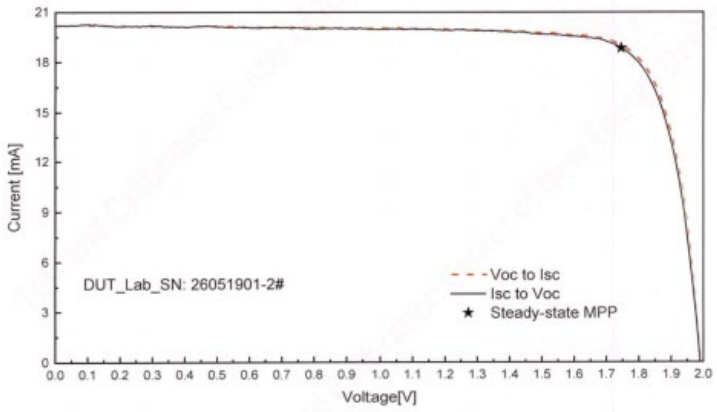

Fig.1 I-V curves of the measured sample

Report No. 26TR051902

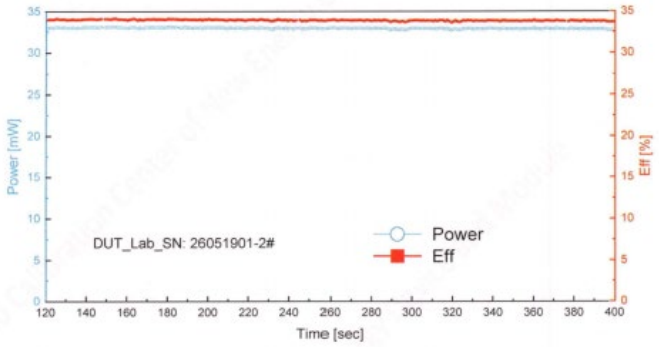

Fig.2 Steady-state maximum power output of the measured sample

Supplementary Fig. 34 Certification of forward/reverse-scan efficiency and stabilized efficiency of one **S2**-based TSCs measured by Shanghai Institute of Microsystem and Information Technology, Chinese Academy of Sciences (SIMIT).

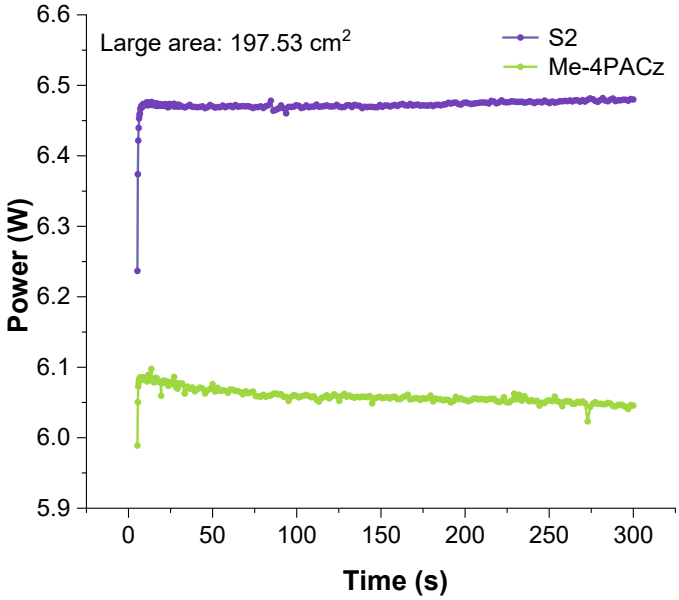

Supplementary Fig. 35 Maximum power point tracking (MPP) tracking over 300 seconds for the highest-efficiency TSCs fabricated by slot-die coating based on **S2** and Me-4PACz SAMs. The average performance parameters over the last 300 s: V = 1.746 V, I =3.710 A, P = 6.479 W for **S2**-based devices, V = 1.728 V, I = 3.500 A, P = 6.047 W for Me-4PACz -based devices.

Fraunhofer ISE

CalLab PV Cells

10003051TSE0525F5d

4. Messergebnis
Measurement results

Diese Messergebnisse beziehen sich ausschließlich auf das oben genannte Messobjekt. *These results exclusively refer to the measurement object above.*
Kennlinienparameter des Messobjektes unter Standardtestbedingungen (STC) / *IV-curve parameter under Standard Testing Conditions (STC)* :

		Vorwärtsrichtung / *forwards scan direction*	Rückwärtsrichtung / *reverse scan direction*	steady state MPP
V_{oc}	=	(1979 ± 20) mV	(1978 ± 20) mV	
I_{SC} (Ed.2 - 2008)	=	(3862 ± 85) mA	(3860 ± 85) mA	
I_{MPP}	=	3673 mA	3689 mA	(3709 ± 137) mA
V_{MPP}	=	1721 mV	1719 mV	(1730 ± 35) mV
P_{MPP}	=	6321 mW	6341 mW	(6417 ± 300) mW
FF	=	82.7 %	83.0 %	
η	=			(32.6 ± 1.5) %

Ende Seite 5 / *End of page 5*

1

Fraunhofer ISE

CalLab PV Cells

10003051TSE0525F5d

5. Zusatzinformationen
Additional information

Fläche / Area (ap)[1]: A = (196.97 ± 0.20) cm²

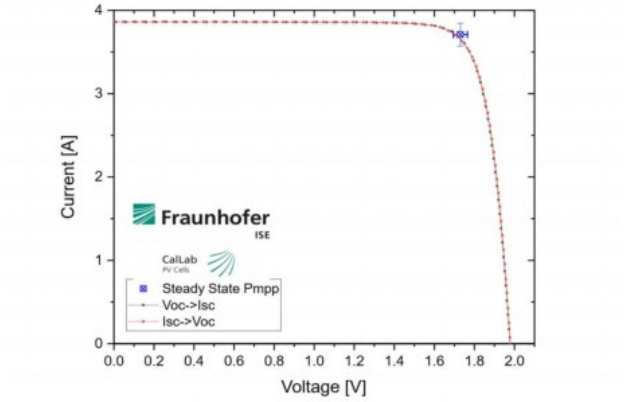

[1] : *(t) = total area, (ap) = aperture area, (da) = designated illumination area /7/*

Angegeben ist jeweils die erweiterte Messunsicherheit, die sich aus der Standardmessunsicherheit durch Multiplikation mit dem Faktor *k*=2 ergibt. Sie wurde gemäß dem "Guide to the expression of Uncertainty in Measurement" ermittelt. Sie entspricht bei einer Normalverteilung der Abweichungen vom Messwert einer Überdeckungswahrscheinlichkeit von 95%.
The expanded measurement uncertainty resulting from the standard measurement uncertainty multiplied with a factor k=2 is specified. The calculation was carried out according to the "Guide to the expression of Uncertainty in Measurement". The value corresponds to a Gaussian distribution denoting the deviations of the measurement value within a probability of 95%.

2

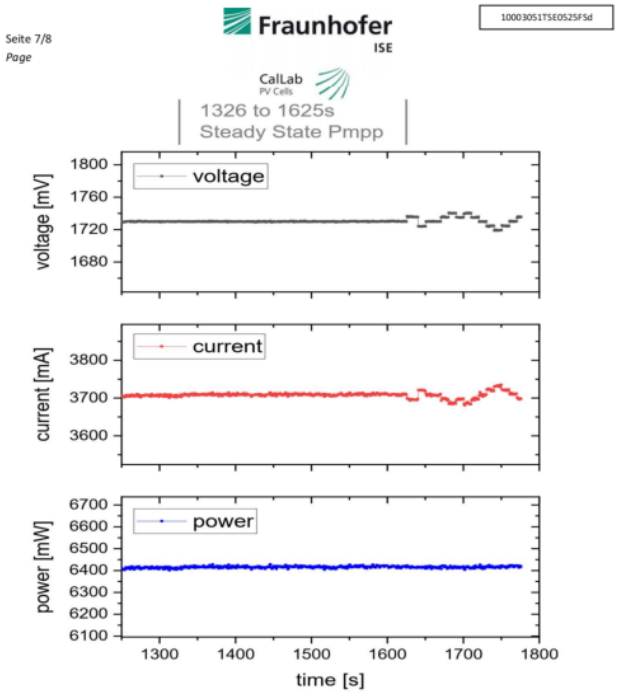

1

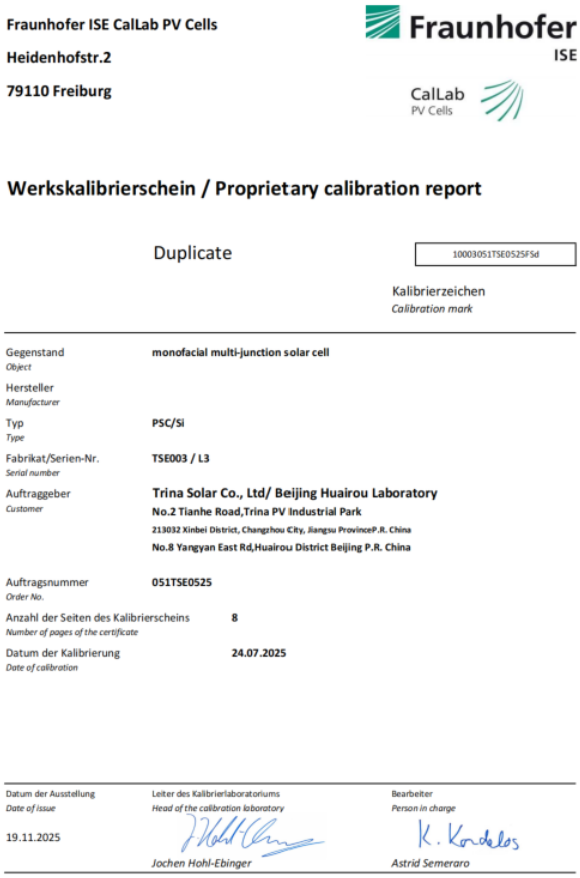

Fraunhofer ISE CalLab PV Cells
Heidenhofstr.2
79110 Freiburg

Fraunhofer ISE
CalLab PV Cells

Werkskalibrierschein / Proprietary calibration report

Duplicate

10003051TSE0525FSd

Kalibrierzeichen
Calibration mark

Gegenstand *Object*	**monofacial multi-junction solar cell**
Hersteller *Manufacturer*	
Typ *Type*	**PSC/Si**
Fabrikat/Serien-Nr. *Serial number*	**TSE003 / L3**
Auftraggeber *Customer*	**Trina Solar Co., Ltd/ Beijing Huairou Laboratory** **No.2 Tianhe Road,Trina PV Industrial Park** **213032 Xinbei District, Changzhou City, Jiangsu ProvinceP.R. China** **No.8 Yangyan East Rd,Huairou District Beijing P.R. China**
Auftragsnummer *Order No.*	**051TSE0525**
Anzahl der Seiten des Kalibrierscheins *Number of pages of the certificate*	**8**
Datum der Kalibrierung *Date of calibration*	**24.07.2025**

Datum der Ausstellung *Date of issue*	Leiter des Kalibrierlaboratoriums *Head of the calibration laboratory*	Bearbeiter *Person in charge*
19.11.2025	*Jochen Hohl-Ebinger*	*Astrid Semeraro*

2

3 **Supplementary Fig. 36** Certification of *J-V* curve and stabilized efficiency output of

1 TSCs (~196.67 cm^2) by Fraunhofer ISE CalLab.

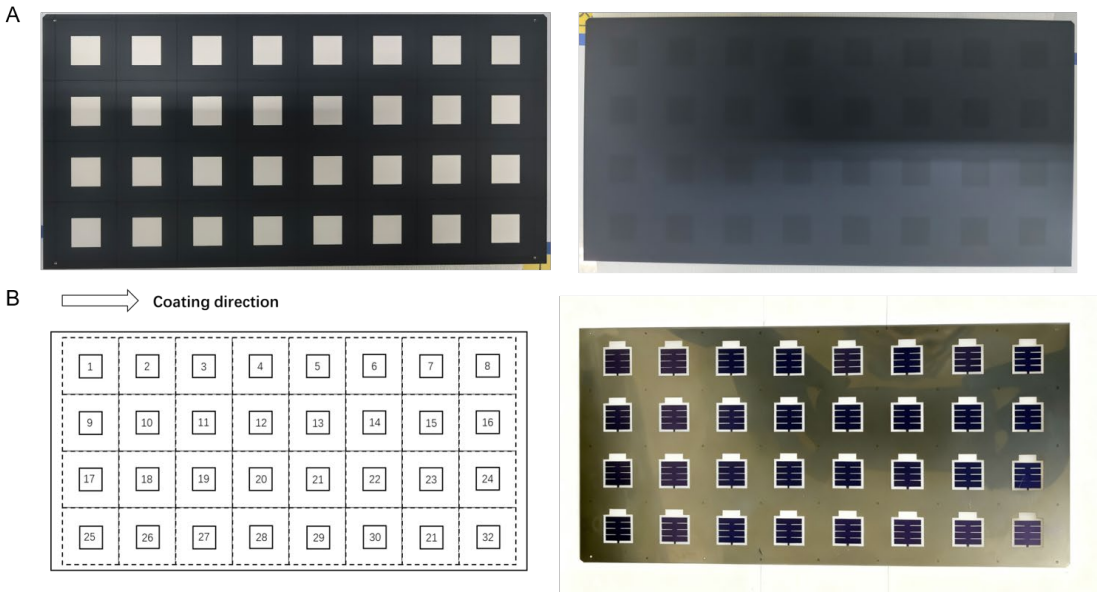

Supplementary Fig. 37 (A) Photographs of the front side and backside of a 210 mm half-cut silicon bottom cell used for fabricating small-area tandem cells. (B) The coating direction and cell numbering for perovskite layer deposition on the same 210 mm half-cut silicon bottom cell, the photograph of completed tandem cells is shown in the right.

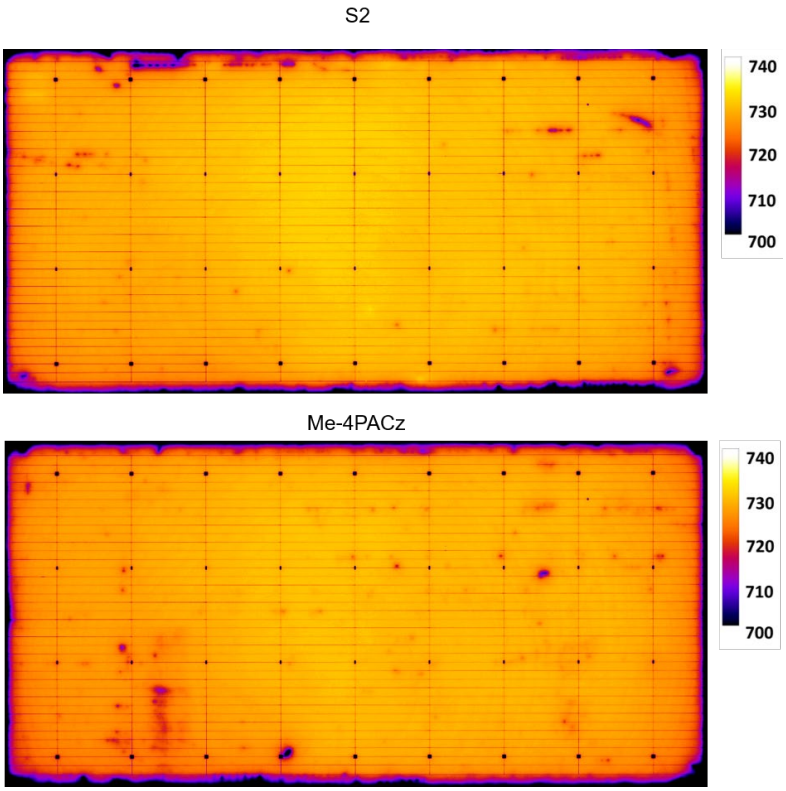

Supplementary Fig. 38 PL mapping of iV_{OC} on the silicon bottom cell of a large-area TSCs based on **S2** and Me-4PACz.

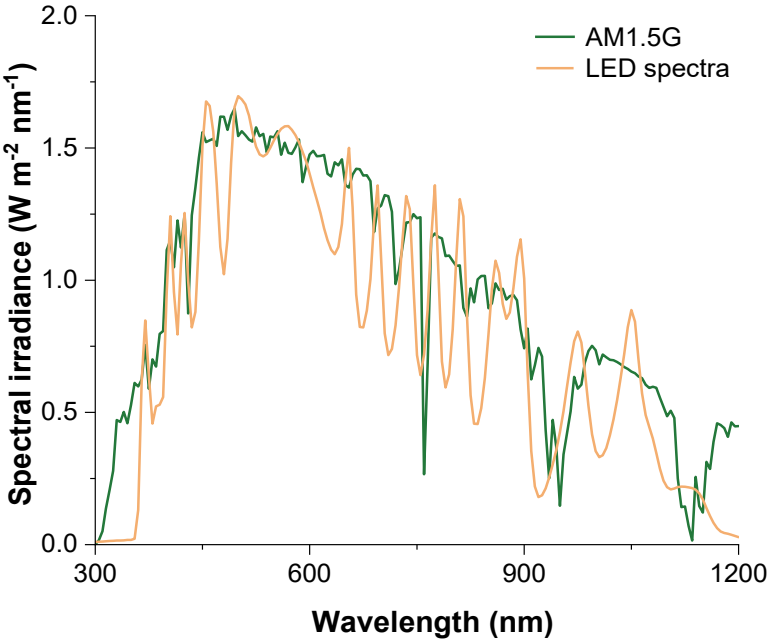

Supplementary Fig. 39 Simulated solar spectrum for stability test.

Supplementary Table 1. XPS-derived P: In atomic ratios for different SAMs on ITO substrates. The coverage factor was calculated from the P 2*p* to In 3*d* peak area ratio before and after washing with different cycles of ethanol.

SAM	Condition	P 2*p* area	In $3d_{3/2}$ area	Coverage factor ($*10^{-3}$)
Me-4PACz	fresh	3870.59	447177.09	8.656
	wash 1 cycle	3883.10	575273.47	6.750
	wash 2 cycles	3531.36	565847.93	6.241
	wash 3 cycles	3387.69	582478.45	5.816
SC	fresh	4703.95	478752.51	9.825
	wash 1 cycle	3525.58	471264.55	7.481
	wash 2 cycles	2844.09	444396.68	6.400
	wash 3 cycles	3158.83	519960.77	6.075
S2	fresh	4106.86	354950.31	11.57
	wash 1 cycle	3800.56	362611.07	10.48
	wash 2 cycles	4688.69	456162.15	10.28
	wash 3 cycles	4386.83	440376.19	9.962

Supplementary Table 2. Photovoltaic parameters of the best-performing n-i-n devices based on different SAMs.

SAM	Direction	J_{SC} (mA cm^{-2})	V_{OC} (V)	FF (%)	PCE(%)
Me-4PACz	reverse	20.93	1.248	79.32	20.72
	forward	20.92	1.248	78.33	20.45
SC	reverse	20.89	1.262	80.34	21.18
	forward	20.89	1.26	79.74	20.99
S2	reverse	20.92	1.284	83.9	22.54
	forward	20.91	1.285	83.7	22.49

Supplementary Table 3. Statistical comparison of photovoltaic parameters under reverse scan of n-i-n devices fabricated with different SAMs.

Me-4PACz			
V_{OC} (V)	J_{SC} (mA/cm^2)	FF (%)	PCE (%)
1.248	20.93	79.32	20.72
1.243	20.85	78.91	20.45
1.231	20.89	79.12	20.35
1.241	20.85	78.2	20.23
1.235	20.83	79.17	20.37
1.229	20.87	78.57	20.15
1.245	20.9	78.88	20.52
1.242	20.91	78.49	20.38
1.225	20.84	78.8	20.12
1.229	20.86	79.34	20.34
1.238	20.95	79.33	20.58
1.240	20.94	79.01	20.52
1.237	20.89	78.93	20.39
SC			
V_{OC} (V)	J_{SC} (mA/cm^2)	FF (%)	PCE (%)
1.262	20.89	80.34	21.18
1.259	20.89	80.01	21.04
1.256	20.91	80.21	21.07
1.251	20.88	79.77	20.84
1.249	20.83	79.89	20.78
1.248	20.86	79.92	20.81
1.255	20.92	80.31	21.09
1.247	20.84	80.08	20.81
1.251	20.92	79.56	20.82
1.252	20.87	79.11	20.67
1.246	20.86	79.23	20.59
1.251	20.9	79.43	20.77

1.251	20.88	79.775	20.835
S2			
V_{OC} (V)	**J_{SC} (mA/cm^2)**	**FF (%)**	**PCE (%)**
1.284	20.92	83.9	22.54
1.273	20.88	83.12	22.09
1.288	20.83	83.54	22.41
1.271	20.91	83.21	22.11
1.265	20.85	82.95	21.88
1.263	20.84	82.76	21.78
1.280	20.91	83.71	22.40
1.275	20.86	82.97	22.07
1.272	20.85	83.58	22.17
1.284	20.87	82.97	22.23
1.272	20.89	83.08	22.08
1.266	20.9	83.01	21.96
1.274	20.88	83.23	22.14

1

Supplementary Table 4. Photovoltaic parameters of the best-performing lab-scale TSCs based on different SAMs.

SAM	Direction	J_{SC} (mA cm^{-2})	V_{OC} (V)	FF (%)	PCE (%)
Me-4PACz	reverse	20.40	1.972	80.7	32.46
	forward	20.39	1.970	79.9	32.08
SC	reverse	20.33	1.983	81.9	33.02
	forward	20.34	1.982	79.8	32.17
S2	reverse	20.30	1.994	84.70	34.29
	forward	20.30	1.994	84.71	34.18

Supplementary Table 5. Photovoltaic parameters of the best-performing large-area TSCs based on different SAMs.

SAM	Direction	J_{SC} (mA cm^{-2})	V_{OC} (V)	FF (%)	PCE(%)
Me-4PACz	reverse	19.81	1.959	79.8	30.97
	forward	19.80	1.951	77.7	30.02
S2	reverse	19.73	1.980	84.0	32.81
	forward	19.71	1.976	83.8	32.63

Supplementary Table 6. Summary of reported photovoltaic performance parameters for 210×105 mm^2 (half-cut) monolithic perovskite/silicon tandem solar cells. Note that the 210 mm half-wafer size represents the dominant industrial standard for both present and forthcoming production.

Entity/Research Group	Total Area (cm^2)	Active Area (cm^2)	Certified PCE (%)	Certification Agency	Reference
Maxwell	220.5	Unknown	32.38	NIM	https://www.maxwell-gp.com/news/2032/[2]
Auner	220.5	Unknown	32.29	NPVM	https://mp.weixin.qq.com/s/mqhjDW4lMfq-XmIshU7SQQ[3]
JA Solar	220.5	Unknown	31.27	NPVM	https://news.solarbe.com/202509/23/50009204.html[4]
Tongwei	220.5	Unknown	27.52	/	https://www.tongwei.com/index.php/news/detail/169000.html[5]
Trina	220.5	Unknown	31.1	ISE-Callab	https://www.trinasolar.com/cn/resources/newsroom/thu-20250410-2000/[6]
Soochow University	220.5	200	31.0	CPVT	*Science,* 2026, 393, 200. [7]
Soochow University	220.5	207.87	30.60	NPVM	*Nature Energy*, 2026, Doi: 10.1038/s41560-026-02116-4[8]
This work	**220.5**	**196.97**	**32.6**	**ISE-Callab**	**This work**

Maxwell, *Suzhou Maxwell Technologies Co., Ltd.*
Auner, *Auner Optoelectronic Technology Co., Ltd.*
JA Solar, *JA Solar Technology Co., Ltd.*
Tongwei, *Tongwei Co.,Ltd.*
Trina, *Trina Solar Co., Ltd.*
NPVM, *Chinese National Photovoltaic Industry Measurement and Testing Center (China)*
NIM, *National Institute of Metrology (China).*
CPVT, *National Center of Inspection on Solar Photovoltaic Products Quality (China).*
ISE-Callab, *Calibration Laboratory of the Fraunhofer Institute for Solar Energy Systems ISE (Germany).*

Supplementary Table 7. Statistical comparison of photovoltaic parameters under reverse scan of lab-scale TSCs fabricated with different SAMs

Me-4PACz			
V_{OC} **(V)**	J_{SC} **(mA/cm^2)**	**FF (%)**	**PCE (%)**
1.972	20.4	80.7	32.46
1.975	20.33	79.13	31.77
1.964	20.27	80.76	32.15
1.971	20.2	79.21	31.54
1.958	20.28	79.17	31.44
1.981	20.26	79.71	31.99
1.963	20.31	80.5	32.09
1.969	20.46	79.49	32.02
1.971	20.32	78.98	31.63
1.967	20.24	79.3	31.57
1.978	20.27	80.5	32.28
1.968	20.41	78.64	31.59
1.972	20.35	79.52	31.91
1.966	20.41	80.01	32.10
1.969	20.27	79.43	31.70
1.958	20.38	79.36	31.67
1.97	20.33	80.13	32.09
1.961	20.31	79.05	31.48
1.959	20.24	80.51	31.92
1.965	20.39	80.17	32.12
SC			
V_{OC} **(V)**	J_{SC} **(mA/cm^2)**	**FF (%)**	**PCE (%)**
1.983	20.33	81.9	33.02
1.981	20.34	80.62	32.48
1.977	20.27	79.99	32.06
1.978	20.24	79.54	31.84
1.977	20.42	80.55	32.52

1.966	20.44	79.94	32.12
1.979	20.37	81.38	32.81
1.978	20.33	80.3	32.29
1.981	20.28	81.12	32.59
1.985	20.4	79.62	32.24
1.973	20.31	79.89	32.01
1.968	20.32	79.46	31.78
1.968	20.39	80.22	32.19
1.982	20.36	81.38	32.84
1.983	20.39	80.86	32.69
1.984	20.36	80.9	32.68
1.964	20.34	79.43	31.73
1.97	20.36	80.84	32.42
1.984	20.25	79.62	31.99
1.974	20.27	82.51	33.01
S2			
V_{OC} (V)	**J_{SC} (mA/cm^2)**	**FF (%)**	**PCE (%)**
1.994	20.3	84.71	34.29
1.990	20.31	83.88	33.90
1.991	20.19	84.58	34.00
1.989	20.33	83.57	33.79
1.978	20.32	83.96	33.75
1.985	20.32	84.60	34.12
1.986	20.24	84.14	33.82
1.991	20.37	83.74	33.96
1.983	20.42	83.41	33.78
1.993	20.35	84.37	34.22
1.995	20.34	83.75	33.98
1.996	20.41	83.59	34.05
1.991	20.26	83.79	33.80
1.983	20.39	84.23	34.06
1.992	20.27	83.8	33.84
1.99	20.33	82.99	33.58

1.988	20.27	83.98	33.84
1.998	20.41	83.58	34.08
1.992	20.38	82.58	33.52
1.991	20.35	82.80	33.55

1

Supplementary Table 8. Statistical comparison of photovoltaic parameters under reverse scan of large-area TSCs fabricated with different SAMs.

Me-4PACz			
V_{OC} **(V)**	J_{SC} **(mA/cm^2)**	**FF (%)**	**PCE (%)**
1.959	19.81	79.8	30.97
1.951	19.73	80.22	30.88
1.958	19.72	80.14	30.94
1.932	19.74	79.37	30.27
1.939	19.76	78.31	30.00
1.952	19.68	78.26	30.06
1.945	19.69	77.81	29.80
1.945	19.68	78.19	29.93
1.947	19.72	78.68	30.21
1.953	19.73	78.66	30.31
1.943	19.81	79.65	30.66
1.951	19.75	78.92	30.41
1.945	19.76	77.95	29.96
1.936	19.71	78.71	30.03
1.937	19.65	80.26	30.55
S2			
V_{OC} **(V)**	J_{SC} **(mA/cm^2)**	**FF (%)**	**PCE (%)**
1.98	19.73	84	32.81
1.978	19.69	83.86	32.66
1.983	19.65	84.11	32.77
1.989	19.67	82.88	32.43
1.991	19.72	82.98	32.58
1.982	19.72	83.44	32.61
1.991	19.70	83.62	32.80
1.988	19.73	83.08	32.59
1.983	19.73	83.68	32.74
1.984	19.64	84.1	32.77
1.979	19.72	83.05	32.41
1.975	19.81	82.77	32.38
1.982	19.73	83.28	32.57

1.990	19.68	83.52	32.71
1.984	19.69	83.49	32.62

1

Supplementary references

1 Zhang, B. *et al.* A cross-linked molecular contact for stable operation of perovskite/silicon tandem solar cells. *Science* **390**, 837-842 (2025).

2 https://www.maxwell-gp.com/news/2032/.

3 https://mp.weixin.qq.com/s/mqhjDW4lMfq-XmIshU7SQQ.

4 https://news.solarbe.com/202509/23/50009204.html.

5 https://www.tongwei.com/index.php/news/detail/169000.html.

6 https://www.trinasolar.com/cn/resources/newsroom/thu-20250410-2000/.

7 Shi, W. *et al.* Indium-free perovskite/silicon tandem solar cells with tin oxide recombination layer and electrodes. *Science* **393**, 200-206 (2026).

8 Cao, F. *et al.* High-performance perovskite/silicon tandem solar cells enabled by multifunctional titanium oxynitride recombination layers. *Nat. Energy* (2026).